# ARPES and STM view of heavy-electron quantum criticality: perspectives and challenges

**Stefan Kirchner**

Email: stefan.kirchner@correlated-matter.com
Zhejiang Institute of Modern Physics, Zhejiang University, Hangzhou, Zhejiang 310058, China
Zhejiang Province Key Laboratory of Quantum Technology and Devices, Zhejiang University, Hangzhou 310027, China

**Silke Paschen**

Institute of Solid State Physics, Vienna University of Technology, Wiedner Hauptstr. 8-10, 1040 Vienna, Austria

**Qiuyun Chen**

Science and Technology on Surface Physics and Chemistry Laboratory, Mianyang 621908, China

**Steffen Wirth**

Max Planck Institute for Chemical Physics of Solids, 01187 Dresden, Germany

**Donglai Feng**

State Key Laboratory of Surface Physics and Department of Physics, Fudan University, Shanghai 200433, China
Collaborative Innovation Center of Advanced Microstructures, Nanjing 210093, China

**Joe D. Thompson**

Los Alamos National laboratory, Los Alamos, New Mexico 87545, USA

**Qimiao Si**

Department of Physics and Astronomy and Center for Quantum Materials, Rice University, Houston, Texas 77005, USA

**Abstract.** Angle-resolved photoemission spectroscopy (ARPES) and scanning tunneling microscopy (STM) have become indispensable tools in the study of correlated quantum materials. Both probe complementary aspects of the single-particle excitation spectrum. Taken together, ARPES and STM have the potential to explore properties of the electronic Green function, a central object of many-body theory. In this article, we explicate this potential with a focus on heavy-electron quantum criticality, especially the role of Kondo destruction. We discuss how to probe the Kondo destruction effect

across the quantum critical point using ARPES and STM measurements. We place particular emphasis on the question of how to distinguish between the signatures of the initial onset of hybridization-gap formation, which is the "high-energy" physics to be expected in all heavy-electron systems, and those of Kondo destruction, which characterizes the low-energy physics and, hence, the nature of quantum criticality. We survey recent progress and possible challenges in the experimental investigations, compare the STM and ARPES spectra for several quantum critical heavy-electron compounds, and outline the prospects for further advances.

***Keywords*** — heavy-electron quantum criticality, Kondo destruction, scanning tunneling microscopy, angle-resolved photoemission, hybridization gap

## 1. Introduction

A major objective of quantum materials research is to link observable properties to the nature of quantum mechanical many-body ground states properties and to the characteristics of the excitation spectrum above the ground state. In particular, it aims at understanding and predicting the emergence of novel phases in terms of a minimal set of variables, most notably symmetries and broken symmetries of the ground state and the ensuing classification of the excitation spectrum. The typical energy window commonly involved in the materials of interest can cover a wide range, from a few percent of a meV to several eV. A well-known example is the high-temperature superconductors, which have stimulated research since their discovery more than 30 years ago.

The quest for a unified understanding of different classes of quantum materials has led to the notion of quantum critical points (QCPs) as an economic and powerful way of organizing their phase diagrams [1, 2, 3, 4]. Such continuous zero-temperature phase transitions not only separate different ground states but also give rise to a characteristic behavior; this is the quantum-critical fan, which can extend to comparatively large energies and temperatures. Within this fan, universal scaling behavior is expected up to some material-specific high-energy cutoff. Among the materials classes that are currently attracting particular interest are the cuprates, iron pnictides, pyrochlore iridates, transition metal dichalcogenides, and heavy-electron compounds. An underlying theme of most if not all these materials classes is the tendency of their charge carriers to localize in response to the large effective Coulomb repulsion experienced by the itinerant degrees of freedom. The tendency towards localization gives rise to the bad-metal behavior of these materials.

In the heavy-electron compounds, the primary degree of freedom is the $4f$ electron, which is localized at the lanthanide sites as a result of atomic physics and thus with a characteristic energy of order eV. For the same reason, the wavefunction overlap between the $4f$ orbitals and the band (or $c$) electrons, *i.e.*, the hybridization, is typically small. As a result, the $4f$ electron appears localized at high temperatures or energies in the entire range of phase space as long as the valency of the lanthanide ion remains near its localized limit. In this regime each $4f$ electron contributes a finite amount $\sim \ln N_f$ to the entropy, where $N_f$ is the spin degeneracy. $N_f$ is affected by spin-orbit coupling and the crystal electric fields but as long as $N_f > 1$, the spin entropy remains macroscopically large. As temperature is lowered and the ground state is approached, this entropy needs to be quenched. Evidently, the system possesses several options for releasing this entropy, which lead to different ground states. At zero temperature, the system can transition from one ground state to another upon changing coupling constants in the Hamiltonian. At values of these coupling constants where the ground state energy is non-analytic, the system undergoes a quantum phase transition.

Experiments, however, are performed at nonzero temperatures. The challenge, then, is how to distinguish the approach to different ground states with only a limited, intermediate temperature window accessible to experiment. This task is made even

more difficult given that high-energy properties are largely insensitive to the changes in the coupling constants that take a system through different ground states.

The primary tools for exposing the underlying physics that accompanies the entropy release as the temperature or energy is lowered include spectroscopic methods that can trace excitations over some energy range of interest. For example, spin excitations can be probed with the help of inelastic neutron scattering. Among the various spectroscopic techniques, angle-resolved photoemission spectroscopy (ARPES) and scanning tunneling microscopy (STM) stand out as these allow to most directly trace properties of the one-particle Green function, the basic building block in almost any many-body theory.

In this focused review we survey and compare recent ARPES and STM experiments performed on quantum critical heavy-electron compounds that are located close to ground state instabilites at the border of magnetism with a focus on how critical Kondo destruction [5, 6], *i.e.* the breakdown of Kondo entanglement at zero temperature right at the onset of magnetism, is reflected in ARPES and STM data at elevated temperatures.

The manuscript is organized as follows. After a brief introduction of quantum criticality in heavy-electron systems we recapitulate the relation between APRES and STM measurements and their link with the single-particle Green function. We then discuss recent STM measurements on $YbRh_2Si_2$, a heavy-electron antiferromagnet that features a Kondo-destruction QCP as a function of applied magnetic field, before turning to high-resolution ARPES measurements on the Cerium-115 family that consists of $CeMIn_5$ ($M$=Co,Rh,Ir). We close with an outlook on current challenges and future directions.

## 2. Quantum criticality

In stoichiometric heavy-electron compounds containing, *e.g.*, Ce or Yb elements, $4f$ electrons in a partially-filled $4f$ shell are strongly correlated. The spin-orbit interaction and the crystal electric field generated by the ligands surrounding the Ce or Yb ion in the crystalline environment reduce the degeneracy of the $4f$ shell. Most commonly, the lowest-lying atomic $4f$-levels correspond to a Kramers doublet. As a result, the $4f$ electrons behave as a lattice of effective spin-1/2 local moments. This leads to an effective description in terms of the Kondo lattice Hamiltonian:

$$H_{\rm KL} = H_0 + \sum_{ij} I_{ij} \mathbf{S}_i \cdot \mathbf{S}_j + \sum_i J_K \mathbf{S}_i \cdot \mathbf{s}_i^c \,, \tag{1}$$

where $H_0 = \sum_{\mathbf{k},\sigma} \varepsilon_{\mathbf{k}} c^\dagger_{\mathbf{k}\sigma} c_{\mathbf{k}\sigma}$ describes the conduction electrons. The RKKY interaction $I_{ij}$ and the Kondo coupling $J_K$ typically are antiferromagnetic, *i.e.*, $I_{ij} > 0$, $J_K > 0$. The competition between these two types of interactions lies at the heart of the microscopic physics for heavy-electron systems [7].

A QCP arises from tuning the ratio of RKKY to Kondo interactions, which is parameterized by the non-thermal control paramater $\delta \equiv T_K^0/I$. Here, $T_K^0 \approx$

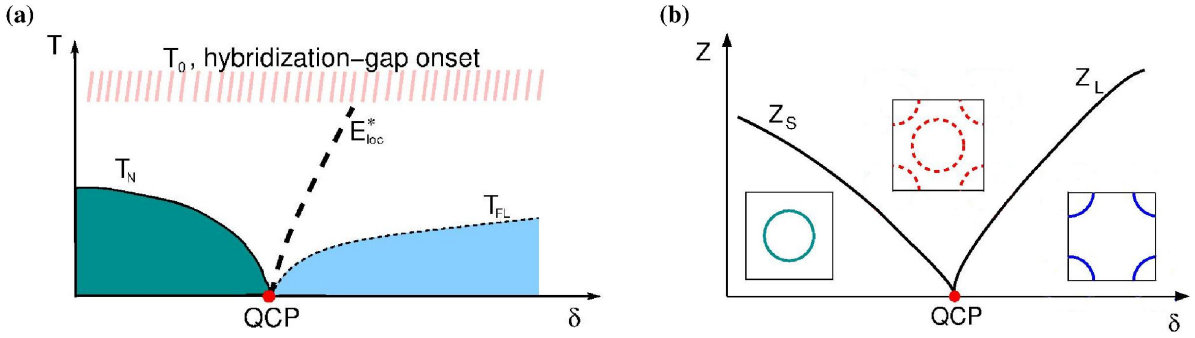


**Figure 1.** Illustrations of basic concepts of Kondo-destruction quantum criticality: (Color online) (a) Local quantum criticality with Kondo destruction, under the variation of the control parameter $\delta$. Here, $T_0$ is a high-energy scale that describes the initial onset of dynamical Kondo correlations and that smoothly evolves across the QCP $\delta_c$. This high-energy scale is reflected in the onset of hybridization-gap formation. The low-energy physics is described in terms of $T_N$ and $T_{FL}$, which are respectively the temperatures for the Néel transition and the crossover into the paramagnetic Fermi-liquid state. This phase diagram also involves the Kondo-destruction energy scale $E^*_{\rm loc}$, which characterizes the Kondo destruction. The $E^*_{\rm loc}$ line divides the phase diagram in terms of the flow of the system towards either the Kondo-screened or the Kondo-destruction ground state. (b): The small (left) and large (right) Fermi surfaces, and the associated quasiparticle weights $z_S$ and $z_L$ that are discussed in Section 3. The fluctuating Fermi surfaces (middle) are associated with the QCP.

$\rho_0^{-1} \exp(-1/\rho_0 J_K)$, with $\rho_0$ being the density of states of the conduction electrons at the Fermi energy, whereas $I$ parameterizes the RKKY interaction.

On the paramagnetic side, the ground state is characterized by the amplitude of the *static* Kondo singlets that are formed between the local moments and conduction electron spins [8]. For a Kondo-destruction QCP, this static Kondo-singlet amplitude is continuously suppressed when the system approaches the QCP from the paramagnetic side [5, 9, 10].

As illustrated in Fig. 1, the Kondo-destruction energy scale $E^*_{loc}$ goes to zero as the control parameter $\delta$ approaches the QCP at $\delta_c$ from the paramagnetic side, and the antiferromagnetic order sets in when $\delta$ goes across $\delta_c$. The Kondo destruction goes beyond the Landau framework of quantum criticality. The latter is based on order-parameter fluctuations, which in the present context of antiferromagnetic heavy-electron systems is referred to as a spin-density-wave (SDW) QCP [11, 12, 13].

The Kondo destruction gives rise to a dynamical spin susceptibility which displays unusual scaling at the QCP [5, 10]. This includes a fractional exponent [9, 14, 15] in the singular dependence on frequency ($\omega$) and temperature ($T$), and $\omega/T$ scaling. These features have in fact been observed by inelastic neutron scattering measurements [16, 17].

In the single-particle excitations, the collapse of $E^*_{loc}$ implies a jump of the Fermi surface across the QCP. To contrast this picture with the more traditional scenario of a SDW transition [11, 12, 13], where critical fluctuations are tied to nesting properties

of the Fermi surface, we will refer to quantum criticality exhibiting critical Kondo destruction as *local quantum criticality*. At zero temperature,

- for $\delta > \delta_c$, the Fermi surface is large and is given by the combination of the $4f$ and conduction electrons. A nonzero amplitude of static Kondo singlet will be referred to as defining a *Kondo-screened* ground state. It produces a Kondo resonance, which reflects electronic excitations produced by entanglement of the $4f$-moments with the conduction electrons. The Kondo effect is responsible for the large mass enhancement and a small quasiparticle weight $z_L$ [Fig. 1(b)]. There is a small gap for the single-particle excitations at the small Fermi surface.
- for $\delta < \delta_c$, the Fermi surface is small as determined by the conduction electrons alone. This is because, when the amplitude of the static Kondo singlet vanishes, there is no longer a well-defined Kondo resonance. We refer to this state as a *Kondo-destruction* ground state. However, dynamical Kondo-singlet correlations remain at nonzero frequencies. The lead to the development of $4f$-electron spectral weight near the Fermi energy, which we will refer to as Kondo-resonance-like features. The dynamical Kondo effect (see Ref. [18], as well as earlier discussions in Refs. [10, 9]) still produces a large mass enhancement and a small quasiparticle weight $z_S$ [Fig. 1(b)]. There is a small gap for the single-particle excitations at the large Fermi surface.
- at the QCP, single-particle excitations are gapless and have a non-Fermi-liquid form, both at small and large Fermi surfaces.

### *2.1. High-energy excitations, temperature evolution and mass enhancement*

Figure 1 also contains a high-energy scale $T_0$ which describes *the initial onset* of dynamical Kondo correlations. This scale is generally affected by the presence of higher crystal electric field doublets (or quartets) that together form the $4f$ multiplet [19, 20, 21, 22]. It is important to note that this scale smoothly evolves across the QCP at $\delta_c$. The development of the hybridization gap is associated with the initial onset of dynamical Kondo correlations, as illustrated in Fig. 2, and will appear on both sides of $\delta_c$.

For $\delta > \delta_c$, the temperature evolution of the physical properties reflects the flow of the system towards the Kondo-screened ground state. For instance, the initial onset of dynamical Kondo correlations results in the Kondo-screened ground state; the single-particle excitations develop into fully coherent heavy-quasiparticles at the large Fermi surface as the temperature is lowered below $T_{FL}$, the crossover temperature into the paramagnetic Fermi-liquid state.

For $\delta < \delta_c$, the initial onset of dynamical Kondo correlations still takes place, even though it does *not* in the end lead to a well-defined Kondo resonance and the Kondo-singlet amplitude vanishes in the ground state. Still, as the temperature is further lowered, vestiges of the Kondo effect will be observed at any nonzero temperature. In particular, the effective mass is a dynamical quantity, measuring the dispersion of the

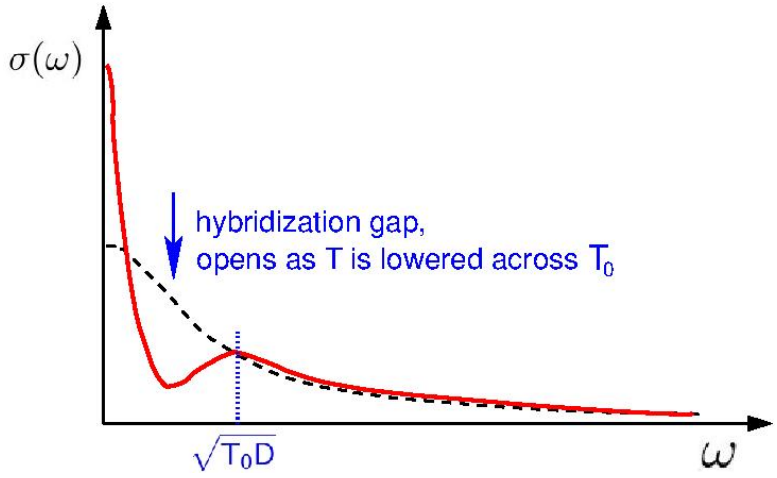


**Figure 2.** Sketch of the optical conductivity $\sigma(\omega)$ for temperatures well above (black dashed line) and well below (continuous red line) the crossover temperature scale $T_0$: (Color online) Here, the lowering of temperature through $T_0$ is accompanied by the onset of the hybridization gap. The characteristic frequency scale for the hybridization gap is $\sqrt{T_0 D}$ (marked by the blue vertical dotted line), where $D$ is an energy scale of the order of the conduction electron bandwidth. At low energies, *i.e.*, for $\omega \ll T_0$ and $T \ll T_0$, and sufficiently far away from quantum criticality (*i.e.* $\delta < \delta_c$ or $\delta > \delta_c$), a pronounced Drude peak reflects the mass enhancement in the Fermi liquid regimes that surround the QCP in the phase diagram [Fig. 1(a)]. The behavior of $\sigma(\omega)$ at high energies, including the hybridization gap, are generic features of heavy-electron systems and are seen throughout the high-energy part of the phase diagram of Fig. 1(a).

Landau quasiparticles, and is enhanced through the dynamical Kondo effect; further discussions of this point can be found in Refs. [18, 10].

### *2.2. Isothermal evolution at low temperatures*

The distinction between the two sides of $\delta_c$ can be sharply made at low temperatures, where well-defined quasiparticles reside at the small Fermi surface for $\delta < \delta_c$ and at the large Fermi surface for $\delta > \delta_c$. At zero temperature, the distinction appears as a sudden jump in the Fermi surface as $\delta$ passes through $\delta_c$. At nonzero but low temperatures, this becomes a crossover. The crossover width increases with increasing temperature. When the crossover width becomes large, the difference between the two sides becomes ambiguous. We will illustrate this point below, especially through the experiments carried out on $YbRh_2Si_2$.

## 3. ARPES, STM, and the single-particle Green function

The unusual $\omega/T$ scaling of the dynamical spin susceptibility sets apart the QCP featuring critical Kondo destruction from the more traditional QCP based on the Landau framework of order-parameter fluctuations, which in the context of heavy-

electron quantum criticality is referred to as an SDW QCP. It means that the dynamical susceptibility $\chi(\omega, T)$, in the regime where scaling ensues, can be scaled to depend on $\omega$ or $T$ only through the combination $\omega/T$. Such scaling has been observed in $CeCu_{6-x}Au_x$ at its antiferromagnetic QCP [23] and indicated for $YbRh_2Si_2$ [24]. Recent measurements of the optical conductivity in thin films of $YbRh_2Si_2$ have demonstrated a singular response in the charge sector with an $\omega/T$ scaling [25]. This is in sharp contrast to an SDW QCP, where only the spin dynamics is expected to be critical, but is in line with critical Kondo destruction [25] as shown in models for the physical $N = 2$ case [26, 27], where $N$ is the spin degeneracy, as well as for dynamical large-$N$ limits [28, 29, 30, 26]. A scaling form of this kind for both the optical conductivity and dynamical spin susceptibility is strongly suggestive of the presence of $\omega/T$ scaling in the single-particle excitations encoded in the one-particle Green function. For a study of this function in the paramagnetic Fermi liquid regime of the Kondo lattice far away from any QCP, in the context of photoemission, see Ref. [31]. This Green function appears in the theoretical description of both ARPES and STM. Both spectroscopic techniques are complementary.

While ARPES directly probes the single-particle excitations as a function of energy and momentum, STM measures a conductance that is local in real space. Both methods are surface sensitive, albeit to different degrees. Furthermore, through variation of the photon energy, the bulk sensitivity of ARPES can be enhanced. By construction, ARPES only probes the occupied part of the single-particle excitation spectrum, which, especially at low temperatures, leads to a sharp cutoff at the Fermi energy [32]. ARPES therefore measures only part of the full spectral function, *i.e.* the imaginary part of the retarded Green function below the Fermi energy. A sketch of the spectral function of a Fermi liquid is shown in Fig. 3 (a). It consists of contributions from the quasiparticle pole and an incoherent background. The quasiparticle pole contributes a factor $z$ to the total area beneath the spectral function, while the incoherent background contributes $(1 - z)$ times the total area. $z$ is commonly called the wave-function renormalization factor and it is inversely proportional to the quasiparticle mass in a Fermi liquid. The evolution of $z$ with tuning parameter is plotted schematically in Fig. 1(b) where we see that $z$ vanishes at a local QCP. The position of the quasiparticle pole as a function of momentum defines the disperion. *Per se*, ARPES is not able to distinguish between the quasiparticle peak and the incoherent part of the spectral function. Provided the energy and momentum resolution is not a limiting factor, however, the characteristic broadening $\delta\epsilon$ of the quasiparticle peak in energy ($\sim |\epsilon_k - E_F|^2$) and with temperature ($\sim T^2$) should be discernible in the momentum distribution curves provided by ARPES. The weight of the quasiparticle peak, in principle, could also be extracted based on the total incoherent part. However, since ARPES only probes occupied states, the complete spectral function is inaccessible. Although, inverse photoemission is in principle able to probe states above the Fermi energy, it is haunted by rather poor energy resolution.

In general, when interpreting ARPES spectra, one needs to keep in mind that in order to relate the photoemission intensity to the spectral function, the one-electron

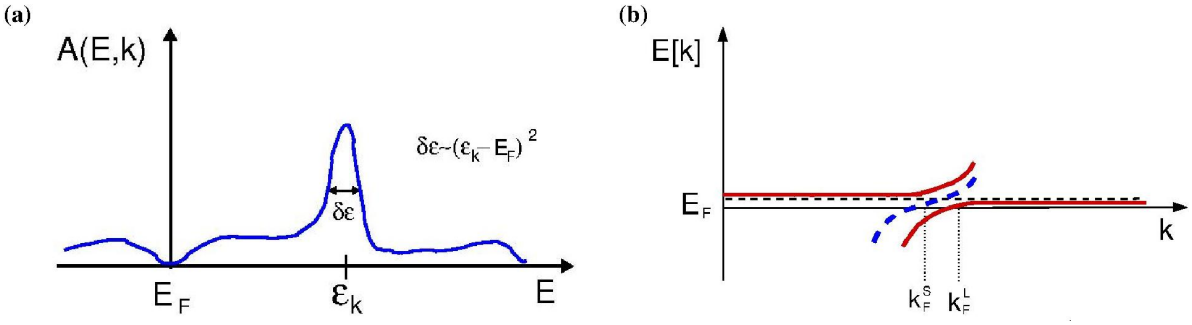


**Figure 3.** Electronic characteristics of the Fermi liquid state of a Kondo lattice: (Color online) (a) Spectral density of a Fermi liquid: The quasiparticle pole at $\epsilon_k$ has a characteristic width $\delta\epsilon$ that increases with the distance from the Fermi energy $E_F$ as $\delta\epsilon \sim |\epsilon_k - E_F|^2$. A similar broadening occurs due to finite-temperature effects. The incoherent part of $A(E, K)$ vanishes at $E_F$. (b) Quasiparticle dispersion in the Fermi liquid to either side of the QCP: $k_F^L$ and $k_F^S$ refer to large and small Fermi surfaces, respectively. Across a Kondo-destruction QCP, the one-electron spectrum is gapless at $k_F^L$ and develops a small gap at $k_F^S$ for $\delta > \delta_c$, and the converse is valid for $\delta < \delta_c$.

dipole matrix element enters, which generally is unknown. In addition, $k_z$ broadening can be important, where $k_z$ is the component of the electron momentum perpendicular to the surface, depending on the photon energy [33, 34].

STM, on the other hand, measures a local-in-real-space conductance. In the linear-response regime, the current-voltage characteristics is related to the local density of states (DOS) of the material under investigation [35, 36]. Therefore, at low bias voltage and temperature, the spatially resolved spectral density can be obtained. As the applied bias voltage shifts the chemical potential at which the local density of states is probed, STM is, unlike ARPES, not confined to only occupied states. It is, however, important to realize that the assumption that the spectral function is independent of the bias voltage has to break down at some sample-dependent value of the bias voltage beyond which the tunneling current can no longer be related to the local density of states. Moreover, the properties of the STM tip, *e.g.* its DOS, may affect the results.

In a Kondo lattice at sufficiently high temperatures, where in first approximation the effect of the RKKY interaction can be ignored, the single-impurity Anderson model is expected to capture the overall physical behavior. This model is given by

$$H_{\mathrm{AND}} = \sum_{\sigma} \varepsilon f_{\sigma}^{\dagger} f_{\sigma} + \sum_{\mathbf{k},\sigma} \varepsilon_{\mathbf{k}} c_{\mathbf{k},\sigma}^{\dagger} c_{\mathbf{k},\sigma} + \frac{U}{2} \sum_{\sigma \neq \sigma'} f_{\sigma}^{\dagger} f_{\sigma'}^{\dagger} f_{\sigma'} f_{\sigma} + \sum_{\mathbf{k},\sigma} \left( V_{\mathbf{k}} f_{\sigma}^{\dagger} c_{\mathbf{k},\sigma} + \mathrm{h.c.} \right) \tag{2}$$

where $f_{\sigma}^{\dagger}$ ($f_{\sigma}$) is the set of local $4f$ electron creation (destruction) operators of spin projection $\sigma$. The conduction electron operators are $c_{\sigma}^{\dagger}$ and $c_{\sigma}$. The band structure of the conduction electrons is encoded in $\varepsilon_{\mathbf{k}}$ and the matrix element $V_{\mathbf{k}}$ that mixes $4f$ and $c$ electrons is referred to as the hybridization. (For the case of the periodic Anderson model in the local moment limit, with the $4f$ electron occupancy being close to unity, it

reduces to the Kondo-lattice model given in Eq. 1 when the charge degrees of freedom of the $4f$ electrons as well as the high-energy part of the conduction electrons are projected out [37, 38].)

STM spectra of single-site Kondo problems possess the structure of Fano resonances [39] and depend on the ratio of tunneling into the Kondo impurity vs tunneling into the embedding host. This ratio is encoded in the so-called Fano parameter. Rigorous derivations of the tunneling current and the form of the Fano parameter are given in [40, 41, 42]. Typically, tunneling occurs predominantly into the conduction band and the corresponding local DOS features the suppression of conduction electron states near the Fermi energy as the Kondo effect develops. The first scanning tunneling studies of dense Kondo systems appeared about a decade ago [43, 44, 45]. The pronounced variation of STM spectra with the type of surface for Kondo lattice compounds is largely due to variations in the Fano parameter, see *e.g.* Fig. 9 for tunneling into a Ce-terminated (a) vs a Co-terminated (b) surface of $CeCoIn_5$. This has been explicitly demonstrated based on mean field and dynamical mean field theory approximations for the Kondo lattice [46, 47, 48, 49]. At sufficiently high temperatures, however, STM spectra in the vicinity of each Ce moment are expected to be similar to those for the single-ion Kondo case. Kondo screening is a predominantly local phenomenon and thus its onset and evolution are easily probed in real space, *i.e.*, via STM. ARPES measurements at similar temperatures, around and above the energy scale $T_0$, provide the band structure $\varepsilon_{\mathbf{k}}$ of the occupied conduction electron states. A flat band near the $4f$ electron atomic level $\varepsilon$ (see Eq. 2), which is far from the Fermi energy, and the formation of a flat band near the Fermi energy induced by the Kondo effect at each Ce moment, reflect the $4f$ electron spectral weight. This can be enhanced using resonant ARPES, see [21].

At (sufficiently) low temperatures, in the Fermi liquid regime to either side of the QCP at $\delta_c$ [Fig. 1(a)], the band structure is shown in Fig. 3(b). For $\delta < \delta_c$, the small Fermi surface prevails and the band structure is that of the black dashed line crossing the Fermi energy $E_F$ at $k_F^S$. Still, incoherent spectral weight, a vestige of incomplete Kondo screening, develops but is ultimately gapped near $k_F^L$. For $\delta > \delta_c$, the Fermi surface incorporates the $4f$ moments and the Fermi wavevector changes from $k_F^S$ at high temperatures (without the $4f$ moments) to $k_F^L$ at low temperatures. On this side of the QCP, any spectral weight near $k_F^S$ is due to incoherent single-particle excitations and is ultimately gapped. In other words, for $\delta > \delta_c$ in the Fermi liquid regime the spectral weight near the black dashed line of Fig. 3(b) has developed a small gap at $k_F^S$. This should in principle be directly detectable via ARPES, provided the energy and momentum resolution is sufficiently high, and low enough temperatures can be reached.

STM on the other hand is a probe of single-electron excitations that are local in real space while the Fermi liquid is a momentum-space concept. As a result, the change from $k_F^S$ to $k_F^L$ has only indirect vestiges in real space. The ensuing difficulties can already be read off from Fig. 3(b): The Fermi liquid is described by a low-energy effective theory and is valid only in the vicinity of $k_F$. (The spectral function is a more general concept but it only assumes a form similar to that shown in Fig. 3(a) in the Fermi liquid regime.)

Fourier transforming the momentum-resolved spectral function to real space necessarily will sum up spectral weight outside of the Fermi liquid regime, where the characteristic broadening that identifies the quasiparticle peak is no longer valid.

One possible way forward is to perform quasiparticle interference experiments to map out the band structure near the Fermi energy [50, 51]. We will return to this possibility in Section 6. Another is to perform isothermal STM measurements at low temperatures through the phase diagram connecting $\delta < \delta_c$ with $\delta > \delta_c$. While this by itself does not provide any direct information on the size of the Fermi surface, it has been recently demonstrated that such a measurement is able to pick up the critical slowing down at the Kondo-destruction energy scale [52], as discussed in the next Section.

## 4. Quantum criticality in $YbRh_2Si_2$

$YbRh_2Si_2$ is a prototype system for local quantum criticality, as illustrated by its temperature ($T$)-magnetic field ($B$) phase diagram [Fig. 4(a)]. Here, the Fermi surface jump and the Kondo-destruction energy scale have been extensively studied through magnetotransport and thermodynamic measurements. At a given temperature, the isothermal Hall coefficient [Fig. 4(b)] and other transport and thermodynamic quantities display a rapid crossover [53, 54, 24]. From these measurements, a $T^*(B)$ line is thus specified in the phase diagram. The full-width at half-maximum (FWHM) of the crossover [Fig. 4(c)] extrapolates to zero in the zero-temperature limit [Fig. 4(d)], which implicates a jump of the Fermi surface across the QCP. It follows that, in the low-temperature limit, at $B < B_c$, the Fermi surface is small.

On the non-magnetic side, $B > B_c$, the mass enhancement diverges as $B$ approaches $B_c$ from above. This has been established by measurements of both the $T$-linear specific-heat coefficient $\gamma$, which is proportional to the effective mass $m^*$, and the $T^2$ coefficient $A$ of the resistivity, which was found to obey the Kadowaki-Woods relation [56]. The divergence of $A$ is shown in Fig. 5.

For $B < B_c$, the mass enhancement is also large. This is compatible with the large $C/T$ measured in the antiferromagnetic state, although to reliably extract $\gamma$ is a challenge because of the interference of the large specific-heat feature at the magnetic transition temperature $T_N$. The mass enhancement can be more reliably extracted from the $A$-coefficient, because the effect of the magnetic transition at $T_N$ on the resistivity is relatively minor. The evolution of the $A$-coefficient with $B$ is consistent with the destruction of the Kondo effect as the QCP is approached from the non-magnetic side as well as the dynamical Kondo effect inside the antiferromagnetic phase.

The effect of increasing temperature on the Hall crossover can be quantified in terms of the ratio of the crossover width to the crossover magnetic field. For $T \gtrsim 0.5$ K, the ratio quickly increases towards unity, as shown in Fig. 4(c). This implies that, for such temperatures, $YbRh_2Si_2$ falls in the quantum critical fluctuation regime already for zero magnetic field. Thus, the single-electron spectral weight will be significant at both the small and large Fermi surfaces. In this temperature range, significant spectral

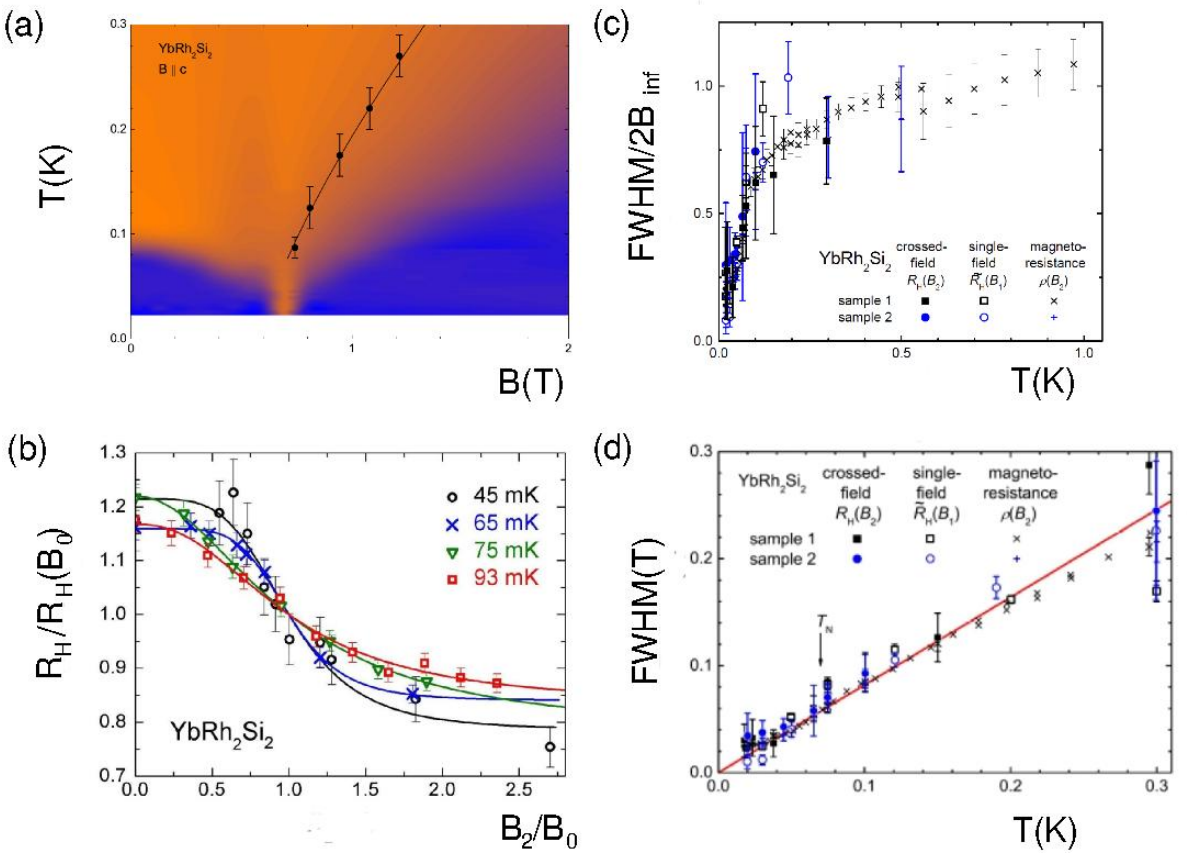


**Figure 4.** Quantum criticality in $YbRh_2Si_2$ (Color online): (a) The temperature vs. field phase diagram of $YbRh_2Si_2$ from [55]. The blue regions marks Fermi liquid behavior, *i.e.*, $\rho(T)-\rho(0) \sim T^2$, while orange indicates the quantum critical area of the phase diagram where $\rho(T)-\rho(0) \sim T^x$, with $x \approx 1$. The continuous line in the quantum critical region is the $E^*$-line as derived from thermodynamic and transport properties. (b) Normalized Hall coefficient across the critical field for different temperatures. The inverse of $R_H$ is a measure of the carrier density. The lower $T$, the sharper is the crossover. At $T = 0$ and $B = B_c$, a jump of $R_H$ corresponds to the sudden localization of $4f$ electrons as $B$ is taken trough $B_c$ from above. From [53]. (c) The full width at half maximum (FWHM) of $R_H$ for different samples and protocols and the magneto-resistance crossover, all centered around $E^*(B)$, vs temperature. From [24]. (d) The "sharpness" of the crossover: The FWHM vanishes in a linear-in-$T$ fashion indicating a jump of $R_H$ at $B_c$ in the zero-temperature limit.

weight is thus to be expected at the large Fermi surface. The ARPES measurements in $YbRh_2Si_2$ at $T > 1$K [58] are consistent with this observation [59].

The temperature evolution of the single-particle excitations in $YbRh_2Si_2$ has been studied by STM measurements, which were first carried out down to 4.6 K in Ref. [60] and were recently extended down to 0.3K [52]. The lattice Kondo effect has been identified with the feature at a particular bias, $-6$meV. The initial onset of this feature takes place near 25K, which corresponds to $T_0^{\rm en}$, an estimate of $T_0$ based on the (spin) entropy $S$ and defined through $S(T_0^{\rm en}/2) = 0.4R\ln 2$, where $R$ is the ideal gas constant, see Table 1. At $B = 0$, the measurements down to $T = 0.3$K show an increase in

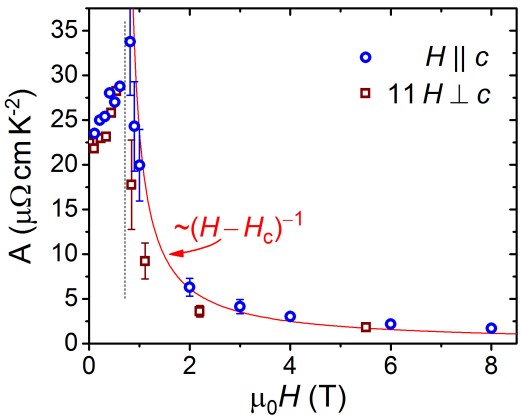


**Figure 5.** Divergence of the A coefficient at the QCP in $YbRh_2Si_2$ (Color online): The effective mass diverges on approach to the critical field $Bc = \mu_0 H_c$ from either side of the QCP. Adapted from Ref. [57].

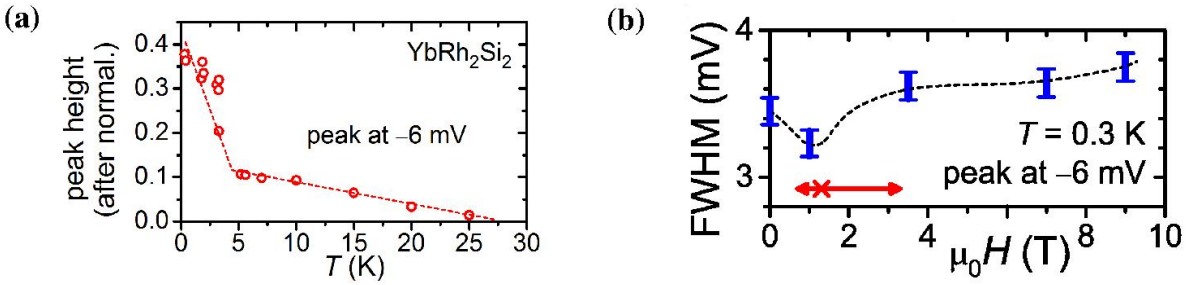


**Figure 6.** STM spectroscopy of the lattice Kondo feature at -6meV in $YbRh_2Si_2$ (Color online): (a) The temperature evolution of the peak height of the -6meV peak. A strong increase in the peak height is observed below 5K. (b) The full width at half maximum (FWHM) of the -6meV peak across the critical field at the base temperature $T = 0.3$K. Note that at this temperature all field values place the system within the quantum critical fan. The critical slowing down at quantum criticality is reflected in a decrease of the peak height near $B^* = \mu_0 H^*(T = 0.3\ \mathrm{K})$. (Data taken from [52]).

the spectral weight [Fig. 6(a)]. This is compatible with the dynamical Kondo effect at nonzero temperatures.

The STM experiments have also determined the isothermal $B$-dependence of the peak width, at the lowest measured temperature $T = 0.3$K. It shows a minimum near $B^*(T = 0.3\mathrm{K})$, as shown in Fig. 6(b). This observation is consistent with a critical slowing down associated with the Kondo-destruction energy scale that was implicated by magnetotransport and thermodynamic meansurements [53, 54, 24]. As such, it represents the most direct evidence so far for the Kondo-destruction quantum criticality based on a single-particle measurement in $YbRh_2Si_2$.

### *4.1. Summary of Section 4*

We now summarize the salient results on $YbRh_2Si_2$ discussed in this section.

*High-energy features:* STM experiments for $YbRh_2Si_2$ at $B = 0$ clearly observe the initial onset of dynamical Kondo correlations around $T_0$, a comparatively high temperature, as expected for any Kondo-lattice system regardless of the nature (Kondo-screened or Kondo destruction) of its ground state. This is consistent with the observation of a hybridization gap in the optical spectrum [61]. As temperature is further lowered below $T_0$, $4f$ electron spectral weight is expected to develop, and this has also been clearly observed.

*Low-energy isotherms:* STM experiments for $YbRh_2Si_2$ have been carried out as a function of magnetic field at $T = 0.3$K. The Kondo-lattice spectral peak shows a critical slowing-down feature at $B^*$, the Kondo-destruction scale previously determined from magnetotransport and thermodynamic measurements. As such, the STM results are consistent with local quantum criticality.

## 5. The Cerium-based 115 family: photoemission vs. tunneling spectroscopy

The Cerium-based 115 family is comprised of compounds $CeMIn_5$ where $M$ =Co, Rh, or Ir. These compounds are stoichiometric and can be grown in a very clean form. All three compounds crystallize in the $HoCoGa_5$ structure type and thus possess tetragonal unit cells. Due to their proximity to quantum criticality, they have contributed considerably to a global understanding of quantum critical heavy-electron materials [62, 63]. While $CeCoIn_5$ and $CeIrIn_5$ under ambient conditions are low-temperature superconductors, $CeRhIn_5$ is an antiferromagnet [64, 65]. For a review, see [66].

### *5.1. $CeIrIn_5$*

$CeIrIn_5$ at ambient pressure is a heavy-electron superconductor with a transition temperature $T_c = 0.40$K. Its specific heat coefficient indicates that $CeIrIn_5$ is less correlated than the other two members of the 115 family [67]. This is in line with an increase in valence fluctuations in this compound when compared to $CeCoIn_5$ and $CeRhIn_5$. The superconducting properties of $CeIrIn_5$ have recently attracted attention [68, 69]. To which extend superconductivity in this system is driven by valence fluctuations is still a matter of debate.

In contrast to $CeCoIn_5$ or even $CeRhIn_5$, however, $CeIrIn_5$, has been comparatively less studied by STM and ARPES. Early ARPES studies lead to different conclusions concerning the formation of $4f$-derived flat bands [70, 71]. More recently, a high-resolution ARPES study by Chen et al. mapped out the full bandstructure of $CeIrIn_5$ [72]. Interestingly, this study was able to resolve the complete fine structure of both the $4f^1_{5/2}$ and $4f^1_{7/2}$ peaks in the measured energy-distribution curves (EDCs) and momentum-distribution curves (MDCs), which may be a reflection of the comparatively large valence fluctuations [72].

To the best of our knowledge, no scanning tunneling spectroscopy of $CeIrIn_5$ is available, apart from a STM investigation that focuses on the topography of $CeIrIn_5$

surfaces [45, 73]. Our main focus in this section will therefore be on $CeCoIn_5$ and $CeRhIn_5$.

### *5.2. $CeCoIn_5$*

$CeCoIn_5$ has attracted interest not only for its comparatively high superconducting transition temperature $T_c \sim 2.3$K but also for an overall phenomenology that resembles that of the underdoped cuprates.

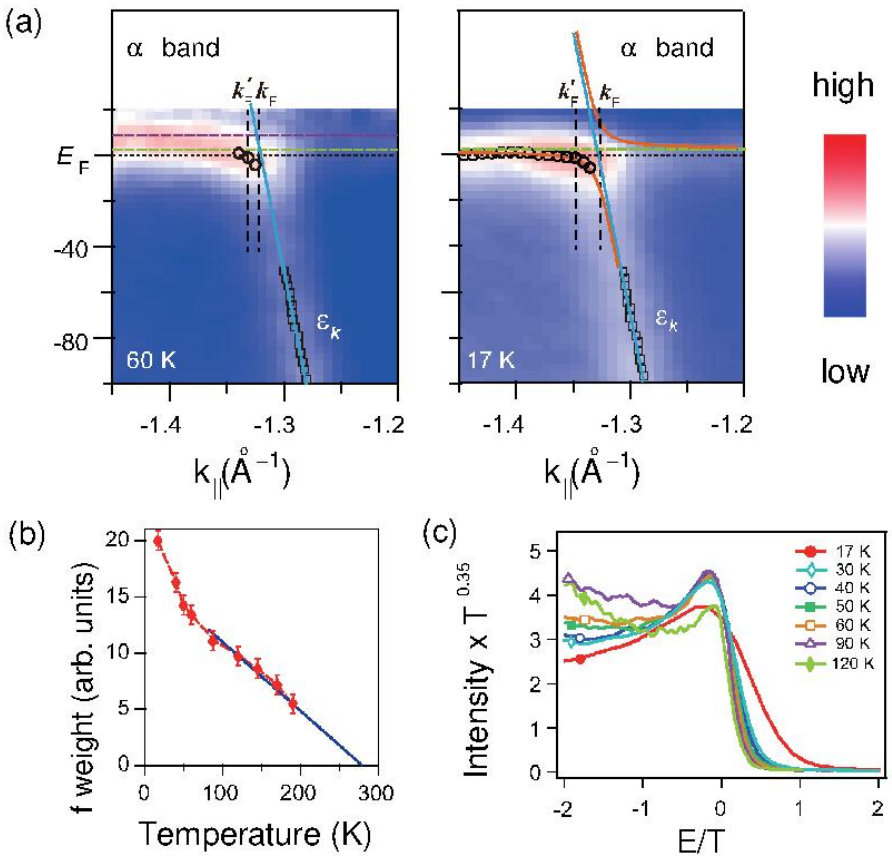


**Figure 7.** ARPES view of the $4f$ electron weight near the Fermi energy in $CeCoIn_5$ (Color online): (a) Evidence for the initial development of hybridization between $4f$ and conduction band $\alpha$ at $T = 60$ and at $T = 17$K after dividing the EDCs by the Fermi-Dirac function. (b) $\omega/T$ scaling of the EDCs near the $\Gamma$ point in an intermediate temperature range and energy range around the Fermi energy $E_F$. (c) Background subtracted $4f$ electron spectral weight transfer near the $\Gamma$ point versus temperature. The EDCs have been integrated over an energy window from -40meV to 2meV. (Data taken from [21]).

The strong interest in $CeCoIn_5$ includes early photoemission studies which, however, have led to contradictory results concerning the localized vs. itinerant nature of the $4f$ electrons [74, 75, 76]. Optical conductivity measurements of $CeCoIn_5$ show the existence of a hybridization gap at high energies which starts forming at comparatively high temperatures [77, 78] and recent STM studies of $CeCoIn_5$ are in line with these

findings [79, 80, 81]. De Haas-van Alphen (dHvA) studies performed at low temperatures indicate that the Fermi surface of $CeCoIn_5$ includes the $4f$ electrons and that therefore the Fermi surface of $CeCoIn_5$ is large [82, 83]. This conclusion is further corroborated by band-structure calculations that treat the $4f$ electrons as fully itinerant [84].

$CeCoIn_5$ under ambient conditions is believed to be located close to an antiferromagnetic QCP of the SDW type and can be tuned to a quantum phase

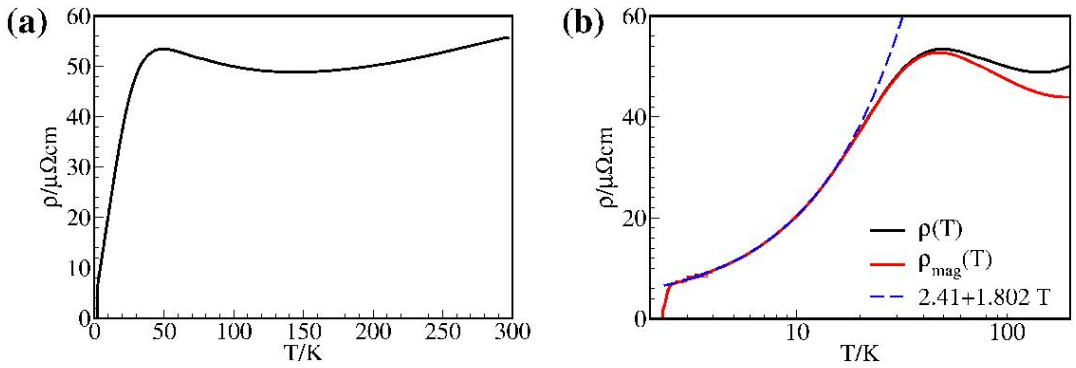


**Figure 8.** Temperature dependence of the resistivity $\rho$ of $CeCoIn_5$ (Color online): (a)$\rho(T)$ in the temperature range from 2.2K to 300K. $\rho$ has a smooth maximum around $T_{\rm coh} \approx 40$K, which defines the coherence temperature $T_{\rm coh}$.

(b) $\rho$ (black continuous line) and the magnetic resistivity $\rho_m$ (red continuous line) in a log-linear plot for temperatures from 2K to 200K. $\rho_m(T)$ is defined as the difference between the resistivity of $CeCoIn_5$ and that of its non-magnetic reference compound $LaCoIn_5$ at temperature $T$. The dashed line represents a linear law fit to $\rho_m(T)$ and shows that $\rho_m(T)$ is linear in $T$ from $T_c$ to approximately 20K.

transition by applying a magnetic field [85, 86, 87]. The STM study by Aynajian et al. also reported an interesting energy-over-temperature ($\omega/T$) scaling of the local conductance of $CeCoIn_5$ which sets in around 60K [79]. It is worth recalling that the STM probes single-electron response while the dynamic spin susceptibility measures the magnetic fluctuation spectrum. As $\omega/T$ scaling is not expected in the dynamical spin susceptibility at a QCP of the SDW type, the observation of dynamical scaling in the local conductance suggests that the SDW nature applies, at least at ambient conditions, only at asymptotically low energies. In any case, the observation of $\omega/T$ scaling does appear to be in line with the linear-in-temperature behavior of the resistivity below 20K as shown in Fig. 8 [64]. Further support in favor of such an $\omega/T$ scaling in $CeCoIn_5$ for the single-particle excitations near the $\Gamma$ point has come from a recent high-resolution ARPES study [21].

The ARPES study by Chen et al. reported the first 3D Fermi-surface mapping of $CeCoIn_5$ and provided a measurement of the full band structure of this heavy-electron system [21]. Due to the large temperature range of the study from 14K to 310K, Chen et al. were able to demonstrate that the formation of the $4f$-derived flat band sets in at temperatures far above the coherence temperature. This finding is significant, although not entirely unexpected. It demonstrates not only the slow evolution of the Kondo screening process but also the likely role of a Kondo effect on the excited crystal

field levels [21, 88]. It also calls into question the inferred temperature-independence of the Fermi surface in $YbRh_2Si_2$ by Kummer et al. which is based on a temperature window from 1K to 100K [58]. Also in contrast to this conclusion about $YbRh_2Si_2$, an earlier laser-based ARPES study of $YbRh_2Si_2$ reported a $T$-dependent bandstructure below 100K [89]. High-resolution ARPES results on $CeCoIn_5$ that are largely compatible with those of Chen et al. [21] have also been reported by Jang et al. [90]. Though ARPES measurements on heavy-electron compounds have been a major experimental achievement, care has to be taken when extrapolating to the high-temperature region where the $4f$ electrons have to be localized across the phase diagram, as argued above. In Fig. 7(a) we reproduced the EDCs from [21] for the $\alpha$-band, one of three bands that are part of the (high-temperature) Fermi surface, in the vicinity of its Fermi crossing both for $T = 60$K and $T = 17$K. The data have been divided by the Fermi-Dirac function to access the region (slightly) above the Fermi energy. The dashed lines in Fig. 7(a) indicate the positions of maxima of the main and the first excited CEF-related Kondo-resonance-like features, both of which are taken to be dispersionless. $k_F$ is the Fermi momentum of the conduction electrons without $4f$ participation, *i.e.*, at high temperatures.
In Fig. 7(b), the building-up of spectral weight near the Fermi energy is shown as a function of temperature. This is calculated by integrating the EDCs near the Fermi energy, *i.e.*, from -40meV to 2meV, and after subtracting a flat, temperature-independent overall background. It is worth recalling that the majority of the Kondo-resonance-like features of a Cerium-based system is located above the Fermi energy, a region which is, especially at low $T$, inaccessible to ARPES.

It is instructive to analyze the high-resolution ARPES data of Chen et al. for the temperature-dependent band structure of $CeCoIn_5$ in light of the expectation that the Fermi surface of this compound should contain the $4f$ electrons at sufficiently low temperatures. In other words, in terms of Fig. 1, $CeCoIn_5$ is located on the $\delta > \delta_c$ side of the $E^*_{\rm loc}$ line. Note, however, that Fig. 1 presents one type of specific cut through the global heavy-electron phase diagram [63] and does not contain $CeCoIn_5$ which is believed to be in close proximity to a SDW QCP.
The red continuous line in the right-hand panel of Fig. 7(a) is a fit of the data to the mean field expression for the single level, single band Anderson lattice model. The circles in Fig. 7(a) are obtained from the maximum in the EDCs and interpreted as the dispersion of the quasiparticle band. This leads to the value of $k'_F$, where $k'_F$ is the *projected* zero-temperature Fermi momentum. Such a fit should not be taken too literally. As mentioned above, mean field approaches may, quite generally, be suitable to address the conduction bands at comparatively high energies and temperatures or the low-energy behavior on either the small or the large Fermi volume side in a limited energy range but generically fail to describe the crossover from the high to the low energy/temperature behavior. In addition, there is the general difficulty of constructing the correct mean field theory. The effective model for a multi band system like $CeCoIn_5$

should not be the single level, single band Anderson lattice model. Nonetheless, the mean field construction provides an estimate for the change in Fermi wavevector from its high-temperature value $k_F$ to $k'_F$. If $k'_F = k_F$, the $4f$ electrons remain localized and do not contribute to the Fermi volume. As discussed above and also briefly mentioned in Ref. [91], if the Fermi surface of $CeCoIn_5$ expands from $k_F$ to $k'_F$ as the zero-temperature fixed point is approached, the bandstructure in the vicinity of $E_F$ should resemble that sketched in Fig. 3(a) and the spectral weight close to $k_F$ needs to vanish as $T \to 0$ so that the incoherent spectral weight at the Fermi energy is gapped out. The detection of such a, possibly very small, gap is challenging in view of the limited energy resolution and $k_z$ broadening effects of ARPES experiments as discussed in Section 3. Note that, although it is expected that $k'_F \neq k_F$ in $CeCoIn_5$, results shown in Fig. 7(a) are indicative of a spectral weight increase near and at $k_F$ as the temperature is lowered from $T = 60$K to $T = 17$K. This is most likely not an artifact due to the limited energy resolution of the measurement, indicating that the single-particle excitations are not of the form depicted in Fig. 3(a). This is also corroborated by the strange metal behavior, encoded in an approximately linear-in-temperature dependence of the resistivity over a wide temperature window above the superconducting transition temperature ($T_c \sim 2.3$K) [64]. In Fig. 8, the temperature dependence of the resistivity $\rho$ of $CeCoIn_5$ is shown together with the magnetic resistivity, *i.e.* the difference between the resistivities of $CeCoIn_5$ and its non-magnetic reference compound $LaCoIn_5$.

The ARPES study of Chen et al. also indicated the presence of $\omega/T$ scaling in the EDCs near the $\Gamma$ point in an intermediate temperature range [21]. This is reproduced in Fig. 7(c). Already at around 90K, the EDCs multiplied by $T^{x_{EDC}}$ (with $x_{EDC} \approx 0.36$) collapses on a function depending only on $\omega/T$. This, however, should not be inter-

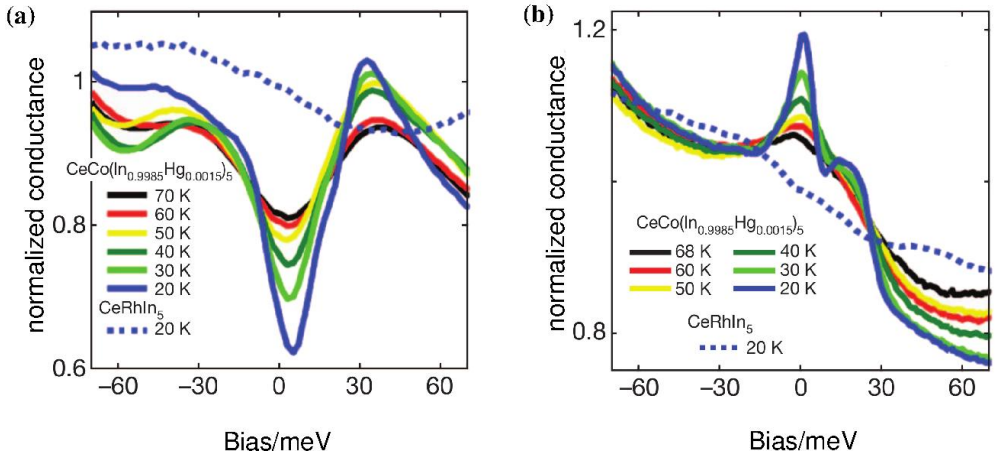


**Figure 9.** Tunneling spectroscopy of $CeCoIn_5$ and $CeRhIn_5$ (Color online): local conductance vs applied bias voltage for different temperatures on (a) Ce-terminated surfaces and (b) Co (respectively Rh)-terminted surfaces. The peak-dip-peak structure in conductance of $CeCoIn_5$ (panel (a)) is typical of a hybridization gap that is not obvious in $CeRhIn_5$, even at the lowest temperature. (Data taken from [79]).

preted as reflecting an $\omega/T$ scaling of all single-particle excitations, which would imply a strict linear-in-$T$ behavior of the resistivity. Indeed, this scaling seems to be confined to the vicinity of the $\Gamma$ point and is absent in the angle-integrated EDCs. Moreover, this peculiar scaling exists only in an intermediate $T$ range and fails below 20K, as shown in Fig. 7(c). This conclusion appears to be compatible with the findings reported in [79], taking into account that tunneling into states with small lattice momenta is favored over tunneling into large-momentum states [36, 92, 93]. This demonstrates that ARPES and STM indeed provide information on the single-particle Green function that can be directly compared to each other. It is, however, noteworthy that the temperature exponents accompanying this $\omega/T$ scaling in the intermediate temperature range from 20K to around 70K differ somewhat depending on the measurement technique. While the STM-derived exponent is $x_{STM} \approx 0.53$, the best fit of the ARPES data was obtained for $x_{EDC} \approx 0.36$. This difference between the ARPES and STM results is most likely due to the dependence of the STM current on the degree of tunneling into $4f$ and $c$ electron states. This dependence is encoded in the Fano parameter.

STM studies on $CeCoIn_5$ (and to a much lesser extent, on $CeRhIn_5$ and $CeIrIn_5$) have been performed by several groups [79, 80, 81, 94, 95, 45]. In Fig. 9(a) and (b), results are shown for the local tunneling conductance of $CeCoIn_5$ very lightly doped with mercury (Hg) as well as $CeRhIn_5$ at different temperatures and on two different surfaces [79]. The Hg-doping induced disorder in $CeCoIn_5$ generates impurity scattering at the dopant sites which in turn can be systematically used to obtain lattice momentum-resolved information of the local DOS through quasiparticle interference (QPI) [50]. This use of QPI to extract the band structure near $E_F$ in the low-temperature limit, however, also has potential shortcomings that were already alluded to in Section 3.

### *5.3. $CeRhIn_5$*

$CeRhIn_5$ is an antiferromagnet with a Néel temperature of $T_N = 3.8$K at ambient pressure and has predominantly localized moments [97]. Under pressure, $T_N$ can be suppressed to zero, thus tuning the system to a QCP at a critical pressure $p_c$. De Haas-van Alphen studies of $CeRhIn_5$ across the QCP display a clear jump at $p_c$, see Fig. 10(a), which implies that the Fermi surface changes discontinuously at the QCP [96]. This compound therefore likely hosts a Kondo-destruction QCP at $\delta_c = p_c$ ($\delta$ was defined in Section 2). This conclusion is further corroborated by an effective mass that tends to diverge on approach to $p_c$, Fig. 10(b), and which reflects the vanishing of the wavefunction renormalization factor $z$, depicted in Fig. 1(b), as the QCP is reached from either above or below $p_c$. This finding is in line with the optical conductivity of $CeRhIn_5$ which has been reported in [98] and which shows the formation of a weak hybridization gap at high frequencies as temperature is lowered below the crossover scale $T_0$.

Despite evidence for the existence of a QCP featuring critical reconstruction of the Fermi surface in $CeRhIn_5$ under pressure, APRES and STM investigations of this

compound are comparatively rare. This is largely due to difficulties in preparing a suitable surface and to the present impossibility of making these measurements under applied pressure. Early non-resonant ARPES investigations of $CeRhIn_5$ reported that the $4f$ electrons in this compound are predominantly itinerant [99], whereas a second non-resonant ARPES study argued that the $4f$ electrons are nearly localized [70].

Scanning tunneling spectroscopy data on Ce- and on Rh-terminated surfaces of $CeRhIn_5$ show no discernible Fano resonances, at least at around 20K [79], see Fig. 9(a)

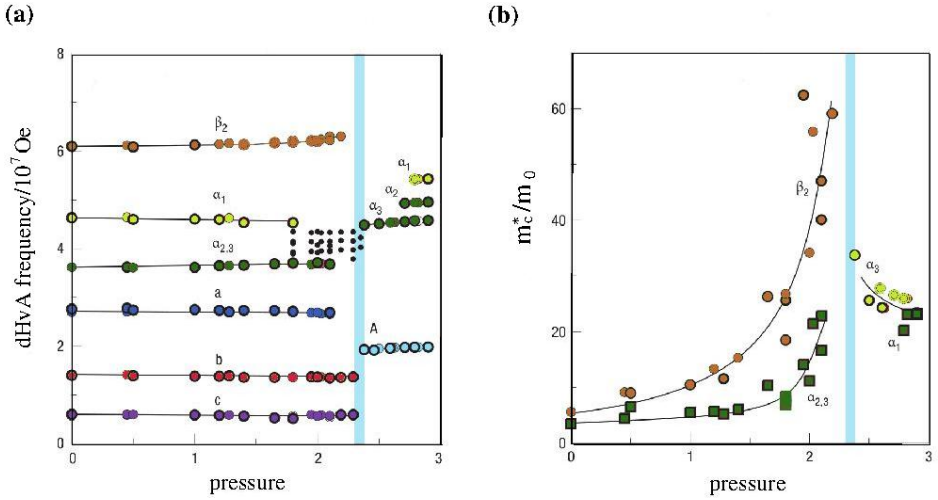


**Figure 10.** De Haas-van Aphen measurements on $CeRhIn_5$ (Color online): (a) Jump of the dHvA frequencies at $p_c$ indicating a reconstruction of the Fermi surface as the QCP is crossed. (b) Diverging effective mass upon approaching $p_c$ from above and below (Data taken from [96]).

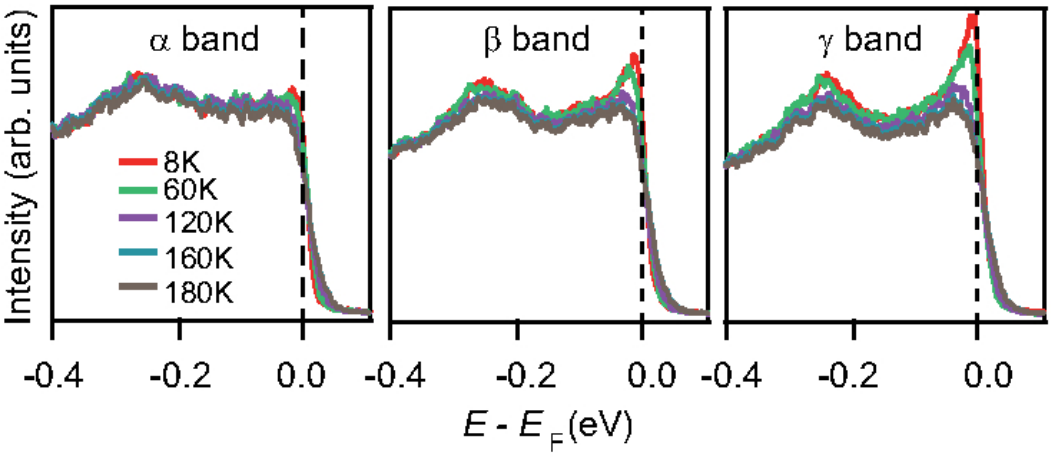


**Figure 11.** EDCs of $CeRhIn_5$ vs temperature (Color online): The energy distribution curves show the evolution of spectral weight with temperature near the Fermi energy $E_F$ for the three bands that cross $E_F$, labelled $\alpha$, $\beta$ and $\gamma$-band. Data were taken at along the $\Gamma$M direction at $k_{\|} = -0.57\mathring{A}^{-1}$ ($\alpha$-band), $k_{\|} = -0.3\mathring{A}^{-1}$ ($\beta$-band), and $k_{\|} = -0.124\mathring{A}^{-1}$ ($\gamma$-band) and with an uncertainty of $\delta k_{\|} \sim 0.03\mathring{A}^{-1}$ for each of the three $k_{\|}$-values. (From [91]).

and (b). Interestingly, these results seem incompatible with high-resolution resonant ARPES data, Fig. 11, which point to the development of the $4f$-electron spectral weight near the Fermi energy, although the weight transfer is much weaker than in $CeCoIn_5$, Fig. 11 [91]. The spectral weight transfer depicted in Fig. 11 for the three bands crossing the Fermi surface also show that, in the temperature range studied, spectral weight transfer occurs mainly near the $\gamma$ band crossing. The difference between the ARPES measurements of [91] and the STM investigation of [79] is likely due to the increased surface sensitivity of STM. One possibility is that the Kondo temperature at the surface is reduced due to the reduced hybridization; a second is that the cleaving process to obtain suitable surfaces appears to be more problematic for $CeRhIn_5$ and $CeIrIn_5$ than for $CeCoIn_5$. In fact, very recent STM results [100] on epitaxially grown $CeRhIn_5$ with well-defined surfaces are very much in line with the ARPES measurements of [91]. As in the case of the STM images of $YbRh_2Si_2$ [see Fig. 6(a)], these data are consistent with the dynamical Kondo effect taking place near the small Fermi surface.

### *5.4. Summary of Section 5*

We close this section by summarizing the status of ARPES and STM investigations in Cerium-based 115 systems, as discussed in this section.

By and large, the existing STM and ARPES results on the Cerium-based 115 family are largely consistent with each other, given the requirements of surface quality and the associated difficulties. The recent high-resolution ARPES investigation of these 115 materials also shows that none of the three compounds follows the low-temperature band-structure expectations of the heavy-electron phenomenology, encoded in Fig. 3(a). This is in line with other measurements, in particular transport measurements which suggest that none is in a Fermi liquid regime in the range where the ARPES measurements were made. Further, the limited energy resolution of state-of-the-art ARPES is still posing a major challenge in the heavy-electron materials class in which the associated energy scales are typically very small.

*High-energy features:* Existing ARPES and STM investigations of the 115 members show the initial onset of dynamical Kondo correlations around the $T_0$ temperature scale [Fig. 1(a)] and the concomitant onset of hybridization-gap formation. This is in line with optical conductivity measurements on these compounds [101]. Comparing ARPES and STM data for the same compound gives complementary results that are compatible with each other, and provide evidence for the existence of the hybridization-gap onset scale $T_0$.

*Low-energy features:* Neither in $CeCoIn_5$ nor $CeRhIn_5$ has ARPES been able to confirm unambiguously the existence of either $k_F^L$ or $k_F^S$. While this may not be surprising due to the limited energy and momentum resolution currently available to ARPES, this finding is also compatible with the absence of Fermi liquid signatures in the investigated temperature range in these compounds; in this range, Fermi liquid signatures are absent as well in transport and thermodynamic properties. Isothermal measurements of dHvA

have shown a sudden reconstruction of the Fermi surface across the pressure-induced QCP in $CeRhIn_5$, which provides strong evidence for Kondo destruction across the QCP.

## 6. Progress, challenge and outlook

### *6.1. High energy Kondo features*

We have stressed that the initial onset of dynamical Kondo correlations or hybridization is expected, at the $T_0$ scale of Fig. 1, for all heavy-electron systems regardless of the nature of their ground states.

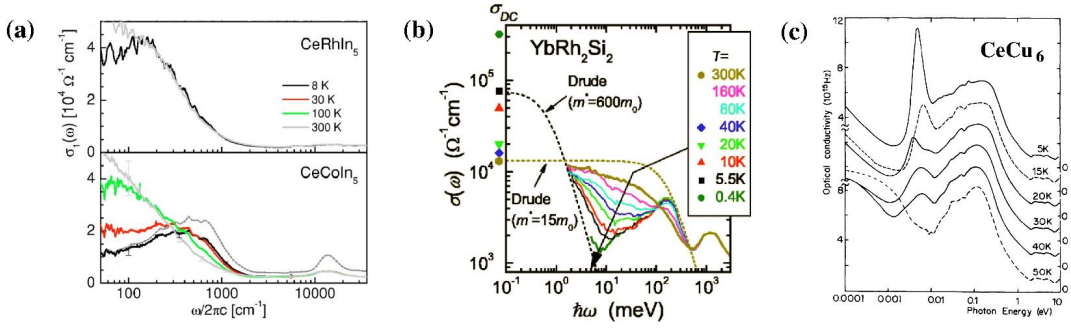


**Figure 12.** Optical conductivity $\sigma(\omega, T)$ and evolution of the hybridization gap (Color online): (a) Although the hybridization gap in $CeRhIn_5$ (top) is overall less pronounced than that in the optical conductivity of $CeCoIn_5$ (bottom), its overall shape and $T$ evolution resembles that of $CeCoIn_5$. (Data taken from [98]). (b) The hybridization gap in $YbRh_2Si_2$ evolves over a large $T$ region, starting well above 100K. As the data are taken at zero external field, the system is located on the $\delta < \delta_c$ side (see section 2) and a Drude peak is therefore expected in $\sigma(\omega, T)$ at small $\omega$ and sufficiently low $T$. (Data taken from [61]). (c) In $CeCu_6$ the optical conductivity develops a hybridization gap at around $\hbar\omega \approx 1$meV below 50K which is flanked towards higher energies by a pronounced peak. (Data taken from [102]).

This scale is evident in $YbRh_2Si_2$ by STM and optical conductivity. Similarly, the formation of a hybridization gap was implicated in $CeRhIn_5$ by optical conductivity measurements [98] and, recently, by STM measurements [100]. Also for $CeCu_6$, which is near a QCP that is accessed by introducing Au-substitution for Cu, a hybridization gap has been observed by optical conductivity [102]. This captures the high-energy $T_0$ scale for the onset of hybridization-gap formation [Fig. 1(a)], and indeed evolves smoothly across the critical substitution $x_c = 0.1$ based on photoemission measurements [103]. The $T_0$ scale is also implicated by recent time-resolved measurements in the critical substitution range [104, 88]. Here, a terahertz irradiation pumps the system and disturbs the correlations between the local moments and conduction electrons. We can expect the underlying Kondo coupling to produce an initial echo at a time corresponding to $\hbar/(k_B T_0)$. Such a finite time scale is indeed observed both away from and at the QCP. Note that the Fermi liquid scale of $CeCu_6$ is 0.2K (see Table 1), which is not accessible by current experiments done at temperature above 1.5K. Nonetheless, it is conceivable

that future experiments may probe not only the echo effect at $\hbar/(k_B T_0)$, but also the scaling time regime much beyond $\hbar/(k_B T_0)$.

Table 1 compiles the of high-temperature and Fermi liquid energy scales of the heavy-electron compounds discussed in this article. The table lists both $T_0^{\rm hyb}$, the initial onset of the hybridization gap, and $T_0^{\rm en}$, based on the (spin) entropy $S$. These two high-energy scales can differ by as much as an order of magnitude, which is not too surprising given that the crossover of Kondo lattice systems from the high-temperature incoherent regime towards the low-temperature coherent/quantum critical/ordered regime is rather broad. This regime can be made even broader when the excited crystal field levels are involved. In practice, we propose to use

$$T_0 = \sqrt{T_0^{\rm hyb}\ T_0^{\rm en}} \tag{3}$$

as a measure of the crossover Kondo scale. Defined in this way, we can infer from Table 1 that $T_0$ is $\sim 62$K in $YbRh_2Si_2$, $\sim 50$K in $CeCoIn_5$, $\gtrsim 25$K in $CeRhIn_5$, and $\gtrsim 13$K in $CeCu_6$.

### *6.2. Isothermal evolution at low temperatures and outlook*

We have discussed in Section 2 that, to assess the nature of quantum criticality (Kondo destruction vs. SDW), the isothermal evolution of quasiparticle spectral weight at low temperatures is particularly informative. In $YbRh_2Si_2$, this has been done through STM measurements as a function of magnetic field at $T = 0.3$ K, and the results [52] support the Kondo-destruction scale that had been inferred from magnetotransport and thermodynamic measurements [53, 54, 24]. Further STM measurements at lower temperatures will clearly be instructive. Whether related STM studies can be carried out in 115 systems is at the present time unclear, because the QCP is realized at a relatively large pressure ($CeRhIn_5$) or possibly at negative pressure ($CeCoIn_5$ and $CeIrIn_5$) [113, 114]. In these latter two cases, applying uniaxial tension might open the possibility of both ARPES and STM studies in a regime that would access their respective QCP. Similar isothermal studies by ARPES appears to be difficult, due to the low temperature that is needed, and also because ARPES cannot be performed in the presence of a magnetic field.

### *6.3. Outlook*

As discussed above (see Section 3), STM is a real space probe and thus generally lacks momentum resolution. It is, however, possible to extract information on the band structure near the Fermi energy using Friedel oscillations that occur near defects [115, 116]. Since STM is a surface probe, QPI only provides a projected bandstructure. Furthermore, the standard approach which is based on Born scattering is known to be insufficient in many cases [117]. This limitation notwithstanding, it will be instructive to obtain bandstructure information through Fourier transform-STM on either side of the QCP to interpret QPI spectra in the quantum critical fan of the QCP.

| | $T_{\rm FL}$/K | $T_0^{\rm hyb}$/K | $T_0^{\rm en}$/K | Reference |
|---|---|---|---|---|
| $YbRh_2Si_2$ | 0.07 | $\sim 160$ | $\approx 24$ | [105, 61, 106] |
| $YbRh_2Si_2$ (B=$B_c$, B$\|$ c) | $< 0.008$ (LMT) | $\sim 160$ | $\approx 24$ | [107, 61, 106] |
| $YbRh_2Si_2$ (B=2T, B$\|$ c) | 0.135 | $\sim 160$ | $\approx 24$ | [57, 61, 106] |
| $CeCoIn_5$ | 0.14 (B=6T) | $\gtrsim 100$ | $\approx 25$ | [108, 98, 64] |
| $CeRhIn_5$ | $< 0.15$ ($p_c = 2.35$GPa, $\mu_0$H=10T) | $\gtrsim 60^{(\dagger)}$ | $\approx 10$ | [109, 91, 62] |
| $CeCu_6$ | 0.2 | $\gtrsim 40$ | $\approx 4$ | [110, 102, 111] |
| $CeCu_{6-x}Au_x$ ($x_c = 0.1$) | $< 0.02$ (LMT) | $\gtrsim 40$ | $\approx 4$ | [112, 102, 111] |

**Table 1.** Characteristic high- and low-temperature scales for several heavy-electron compounds located in the vicinity of quantum criticality. Here, $T_{\rm FL}$ is a temperature scale below which the Landau Fermi liquid $T^2$ resistivity is observed. $T_0^{\rm hyb}$ is a 'high temperature' estimate for the onset of the hybridization gap, and is estimated from the optical conductivity $\sigma(\omega, T)$ (Figs. 2,12) with the exception of $CeRhIn_5$, where existing $\sigma(\omega, T)$ data only indicate that 8K $< T_0^{\rm hyb} <$ 300K [98]. $T_0^{\rm en}$ is a 'low-temperature' estimate of $T_0$ based on the (spin) entropy $S$, using a procedure for the single-impurity Kondo model with constant conduction electron density of states (for which $T_0$=$T_0^{\rm en}$=$T_K^0$): $S(T_0^{\rm en}/2) = 0.4R\ln 2 \approx 0.277R$, where $R = 8314.5$ mJ/(mol K) is the ideal gas constant. (LMT) designates the lowest measured temperature for the electrical resistivity $\rho$.

For $YbRh_2Si_2$ at the critical field, $T_{\rm FL}$ has been estimated from $\rho(T)$ and using the result that $\rho(T) \sim T$ down to the LMT of 8mK [107], marking the listed value to be the upper bound. The hybridization gap onset in $\sigma(\omega < T)$ is assumed to be the same for $0 \le B \le 2$T. Similarly, changes of $T_0^{\rm en}$ are assumed to be small for fields $0 \le B \le 2$T, where the specific heat at around 20K is only weakly field-dependent for $B \le 2T$, see [106].

For $CeRhIn_5$, the QCP is located at $p_c = 2.35$GPa and $H_c$ with $\mu_0 H_c \lessapprox 10$T, see [109].

$^{(\dagger)}$ $T_0^{\rm hyb}$ has been estimated from the ARPES data of [91] for ambient conditions, see also Fig. 11.

For $CeCu_{6-x}Au_{0.1}$, $\rho(T)$ is linear in $T$ down to the LMT 20mK; hence, the listed value is also an upper bound. $T_0^{\rm hyb}$ which is supported by the specific heat data of [112].

The references in this table are arranged such that in each row the first reference provides $T_{\rm FL}$, the second contains estimates for $T_0^{\rm hyb}$ and the third provides results on the low-temperature (spin) entropy.

Critical Kondo destruction is accompanied by a particular kind of $\omega/T$ scaling. Recently, this type of scaling has been demonstrated for the optical conductivity of $YbRh_2Si_2$ thin films grown by molecular beam epitaxy, studied by time-domain THz-transmisson spectroscopy [25]. Epitaxial thin films of members of the 115 family and $CeIn_3$ have been available for some time [118] but STM measurements on these films of $CeCoIn_5$ and $CeRhIn_5$ have only been reported very recently [95, 100]. The observed onset of the hybridization gap in the STM spectrum demonstrates the high-energy $T_0$ scale which, as we have emphasized, is consistent with a Kondo-destruction ground state in $CeRhIn_5$. It will be interesting to see whether a lattice mismatch between substrate and thin film might be used as a substitute for pressure tuning and to establish the range of $\omega/T$ scaling both within the general phase diagram and the type of correlator (single-particle excitations, spin-spin and current-current correlation function, etc.).

We also briefly discussed in Section 3 that the underlying assumption in the interpretation of STM spectra in terms of the equilibrium local DOS is less justified at higher voltages. This may be particularly pertinent near the QCP, where the temperature of the measurement itself is expected to set the only relevant scale [119]. It would be interesting to explore the scaling of spectral density with bias voltage in the nonequilibrium regime which may yet be a further way of unraveling the properties of the underlying QCP [120, 121].

We have so far focused on $YbRh_2Si_2$ and Ce-115 compounds. It will be instructive to carry out measurements of single-electron properties in other candidate heavy-electron materials for Kondo destruction [1, 122, 123, 124]. A case in point is CeNiAsO, in which the antiferromagnetic order has recently been shown to be consistent with that determined by the RKKY interaction of the local moments [125], and transport measurements have suggested the possibility of a Kondo-destruction QCPinduced by either pressure or P-for-As doping [126].

## 7. Conclusion

We have reviewed and compared recent ARPES and STM investigations on heavy-electron materials close to magnetic instabilities with a focus on Kondo-destruction quantum criticality. Real-space and momentum-space spectroscopies combine the power of both methods [127, 128] which has proven to be useful in the study of complex materials such as the cuprate high-temperature superconductors [129, 130]. In the context of Cerium- and Ytterbium-based rare earth intermetallics as well as actinide-based compounds, such a combination seems particularly promising given that much of the excitement and interest generated by these materials derives from the interplay of local and itinerant degrees of freedom; while Kondo screening is primarily a local phenomenon, a possible Fermi-volume increase is best addressed in momentum space. Method-specific constraints, limited energy resolution and the need for very low temperatures in order to resolve a Fermi momentum change across a Kondo-destruction quantum critical point pose unique challenges to both ARPES and STM investigations.

On the other hand, combining ARPES and STM results with other measurements, like resistivity and magnetotransport measurements, neutron scattering and optical conductivity investigations, can provide a consistent picture of Kondo-destruction quantum criticality that emerges as a function of some non-thermal tuning parameter and enables one to locate a specific compound in the general phase diagram of heavy-electron materials. In this regard, we have emphasized the distinction between the spectroscopic properties that reflect the high-energy Kondo physics, such as the formation of the hybridization gap, and those that are capable of probing the nature of quantum criticality, such as low-temperature isothermal measurements across the quantum critical point. The latter has become possible in the STM measurements of $YbRh_2Si_2$, which corroborates the Kondo-destruction energy scale that had been extracted by isothermal magnetotransport and thermodynamic measurements. In $CeRhIn_5$, strong evidence for Kondo destruction in the one-electron excitation spectrum has been provided by quantum oscillation measurements across the critical pressure. It will certainly be instructive to explore further signatures of beyond-Landau quantum criticality in these and other heavy-electron systems.

*Acknowledgements*

We are grateful to the late Elihu Abrahams, Jim Allen, Pegor Aynajian, Ang Cai, Nigel Hussey, Kai Grube, Kevin Ingersent, Johann Kroha, Hilbert von Löhneysen, Yuji Matsuda, Emilian Nica, Jed H. Pixley, Pedro Ribeiro, Rong Yu, Zuo-Dong Yu, Farzaneh Zamani, and Gertrud Zwicknagl for useful discussions. Part of this discussions took place at the 2018 Hangzhou Workshop on Quantum Matter and we thank all participants of the workshop. This work was in part supported by the National Key R&D Program of the MOST of China, grant No. 2016YFA0300200 (S.K., Q.C., & D.F.), the National Science Foundation of China, No. 11774307 (S.K.), and No. 11874330 (Q.C.) and the Science Challenge Project, grant No. TZ2016004 (D.F.). Work in Vienna was supported by the FWF (Project P 29296-N27). Work at Los Alamos was performed under the auspices of the US Department of Energy, Division of Materials Sciences and Engineering. Work at Rice was in part supported by the NSF (DMR-1920740) and the Robert A. Welch Foundation (C-1411). Q.S. acknowledges the hospitality and the support by a Ulam Scholarship from the Center for Nonlinear Studies at Los Alamos National Laboratory, and the hospitality of the Aspen Center for Physics (NSF, PHY-1607611).

## References

[1] Special issue, Phys. status solidi **250**(3), 417 (2013)
[2] Q. Si, F. Steglich, Science **329**, 1161 (2010)
[3] P. Coleman, A.J. Schofield, Nature **433**, 226 (2005)
[4] S. Sachdev, Quantum Phase Transitions (Cambridge University Press, Cambridge, 1999)
[5] Q. Si, S. Rabello, K. Ingersent, J. Smith, Nature **413**, 804 (2001)
[6] P. Coleman, C. Pépin, Q. Si, R. Ramazashvili, J. Phys. Cond. Matt. **13**, R723 (2001)

[7] S. Doniach, Physica B+ C **91**, 231 (1977)
[8] A.C. Hewson, The Kondo Problem to Heavy Fermions (Cambridge University Press, Cambridge, 1993)
[9] J.X. Zhu, D.R. Grempel, Q. Si, Phys. Rev. Lett. **91**, 156404 (2003)
[10] Q. Si, J.H. Pixley, E. Nica, S.J. Yamamoto, P. Goswami, R. Yu, S. Kirchner, J. Phys. Soc. Jpn. **83**, 061005 (2014)
[11] J. Hertz, Phys. Rev. B **14**, 1165 (1976)
[12] A.J. Millis, Phys. Rev. B **48**, 7183 (1993)
[13] T. Moriya, Spin Fluctuations in Itinerant Electron Magnetism (Springer, Berlin, 1985)
[14] M. Glossop, K. Ingersent, Phys. Rev. Lett. **99**, 227203 (2007)
[15] J.X. Zhu, S. Kirchner, R. Bulla, Q. Si, Phys. Rev. Lett. **99**, 227204 (2007)
[16] A. Schröder, G. Aeppli, R. Coldea, M. Adams, O. Stockert, H. v. Löhneysen, E. Bucher, R. Ramazashvili, P. Coleman, Nature **407**, 351 (2000)
[17] M.C. Aronson, R. Osborn, R.A. Robinson, J.W. Lynn, R. Chau, C.L. Seaman, M.B. Maple, Phys. Rev. Lett. **75**, 725 (1995)
[18] A. Cai, H. Hu, K. Ingersent, S. Paschen, Q. Si, Dynamical Kondo effect and Kondo destruction in effective models for quantum-critical heavy fermion metals (2019). ArXiv:1904.11471
[19] B. Cornut, B. Coqblin, Phys. Rev. B **5**, 4541 (1972)
[20] J. Kroha, S. Kirchner, G. Sellier, P. Wölfle, D. Ehm, F. Reinert, S. Hüfner, C. Geibel, Physica E **18**, 69 (2003)
[21] Q.Y. Chen, D.F. Xu, X.H. Niu, J. Jiang, R. Peng, H.C. Xu, C.H.P. Wen, Z.F. Ding, K. Huang, L. Shu, Y.J. Zhang, H. Lee, V.N. Strocov, M. Shi, F. Bisti, T. Schmitt, Y.B. Huang, P. Dudin, X.C. Lai, S. Kirchner, H.Q. Yuan, D.L. Feng, Phys. Rev. B **96**, 045107 (2017)
[22] S. Pal, C. Wetli, F. Zamani, O. Stockert, H.v. Löhneysen, M. Fiebig, J. Kroha, Phys. Rev. Lett. **122**, 096401 (2019)
[23] A. Schröder, G. Aeppli, E. Bucher, R. Ramazashvili, P. Coleman, Phys. Rev. Lett. (1998)
[24] S. Friedemann, N. Oeschler, C. Krellner, C. Geibel, F. Steglich, S. Paschen, S. Kirchner, Q. Si, Proc. Natl. Acad. Sci. USA **107**, 14547 (2010)
[25] L. Prochaska, X. Li, D.C. MacFarland, A.M. Andrews, M. Bonta, E.F. Bianco, S. Yazdi, W. Schrenk, H. Detz, A. Limbeck, Q. Si, E. Ringe, G. Strasser, J. Kono, S. Paschen, Singular charge fluctuations at a magnetic quantum critical point (2018). ArXiv:1808.02296
[26] A. Cai, Z. Yu, H. Hu, S. Kirchner, Q. Si, Dynamical scaling of charge and spin responses at a Kondo destruction quantum critical point (2019). ArXiv:1902.11293
[27] J.H. Pixley, S. Kirchner, K. Ingersent, Q. Si, Phys. Rev. Lett. **109**, 086403 (2012)
[28] L. Zhu, S. Kirchner, Q. Si, A. Georges, Phys. Rev. Lett. **93**(26) (2004)
[29] S. Kirchner, L. Zhu, Q. Si, D. Natelson, Proc. Natl. Acad. Sci. USA **102**(52), 18824 (2005)
[30] Y. Komijani, P. Coleman, Critical charge fluctuations and $\omega/T$ scaling at the Kondo break-down of heavy fermion systems (2018). ArXiv:1810.08148
[31] T.A. Costi, N. Manini, J. Low Temp. Phys. **126**, 835 (2002)
[32] S. Hüfner, Photoelectron Spectroscopy (Springer-Verlag Berlin Heidelberg, 2003)
[33] V. Strocov, Journal of Electron Spectroscopy and Related Phenomena **130**(1), 65 (2003)
[34] H. Wadati, T. Yoshida, A. Chikamatsu, H. Kumigashira, M. Oshima, H. Eisaki, Z.X. Shen, T. Mizokawa, A. Fujimori, Phase Transitions **79**(8), 617 (2006)
[35] J. Bardeen, Phys. Rev. Lett. **6**, 57 (1961)
[36] J. Tersoff, D.R. Hamann, Phys. Rev. B **31**, 805 (1985)
[37] J.R. Schrieffer, P.A. Wolff, Phys. Rev. **149**, 491 (1966)
[38] F. Zamani, P. Ribeiro, S. Kirchner, New J. Phys. **18**, 063024 (2016)
[39] U. Fano, Phys. Rev. **124**, 1866 (1961)
[40] A. Schiller, S. Hershfield, Phys. Rev. B **61**, 9036 (2000)
[41] O. Újsághy, J. Kroha, L. Szunyogh, A. Zawadowski, Phys. Rev. Lett. **85**, 2557 (2000)
[42] M. Plihal, J.W. Gradzuk, Phys. Rev. B (2001)

[43] P. Aynajian, E.H. da Silva Neto, C.V. Parkera, Y. Huangb, A. Pasupathy, J. Mydosh, A. Yazdani, Proc. Natl. Acad. Sci. **107**, 10383 (2010)
[44] A.R. Schmidt, M.H. Hamidian, P. Wahl, F. Meier, A.V. Balatsky, J.D. Garrett, T.J. Williams, G.M. Luke, J.C. Davis, Nature **465**, 570 (2010)
[45] S. Ernst, S. Wirth, F. Steglich, Z. Fisk, J.L. Sarrao, J.D. Thompson, Phys. Status Solidi B **247**, 247 (2010)
[46] M. Maltseva, M. Dzero, P. Coleman, Phys. Rev. Lett. **103**, 206402 (2009)
[47] P. Wölfle, Y. Dubi, A.V. Balatsky, Phys. Rev. Lett. **105**, 24601 (2010)
[48] J. Figgins, D.K. Morr, Phys. Rev. Lett. **104**, 187202 (2010)
[49] A. Benlagra, T. Pruschke, M. Vojta, Phys. Rev. B **84**, 195141 (2011)
[50] P.G. Derry, A.K. Mitchell, D.E. Logan, Phys. Rev. B **92**, 035126 (2015)
[51] A. Yazdani, E.H. da Silva Neto, P. Aynajian, Annual Review of Condensed Matter Physics **7**(1), 11 (2016)
[52] S. Seiro, L. Jiao, S. Kirchner, S. Hartmann, S. Friedemann, C. Krellner, C. Geibel, Q. Si, F. Steglich, S. Wirth, Nature Comm. **9**, 3324 (2018)
[53] S. Paschen, T. Lühmann, S. Wirth, P. Gegenwart, O. Trovarelli, C. Geibel, F. Steglich, P. Coleman, Q. Si, Nature **432**, 881 (2004)
[54] P. Gegenwart, T. Westerkamp, C. Krellner, Y. Tokiwa, S. Paschen, C. Geibel, F. Steglich, E. Abrahams, Q. Si, Science **315**, 1049 (2007)
[55] J. Custers, P. Gegenwart, H. Wilhelm, K. Neumaier, Y. Tokiwa, O. Trovarelli, C. Geibel, F. Steglich, C. Pépin, P. Coleman, Nature **424**, 524 (2003)
[56] N. Tsujii, H. Kontani, K. Yoshimura, Phys. Rev. Lett. **94**, 057201 (2005)
[57] P. Gegenwart, J. Custers, C. Geibel, K. Neumaier, T. Tayama, K. Tenya, O. Trovarelli, F. Steglich, Phys. Rev. Lett. **89**, 056402 (2002)
[58] K. Kummer, S. Patil, A. Chikina, M. Güttler, M. Höppner, A. Generalov, S. Danzenbächer, S. Seiro, A. Hannaske, C. Krellner, Y. Kucherenko, M. Shi, M. Radovic, E. Rienks, G. Zwicknagl, K. Matho, J.W. Allen, C. Laubschat, C. Geibel, D.V. Vyalikh, Phys. Rev. X **5**, 011028 (2015)
[59] S. Paschen, S. Friedemann, S. Wirth, F. Steglich, S. Kirchner, Q. Si, J. Magn. Magn. Mater. **400**, 17 (2016)
[60] S. Ernst, S. Kirchner, C. Krellner, C. Geibel, G. Zwicknagl, F. Steglich, S. Wirth, Nature **474**, 362 (2011)
[61] S. Kimura, J. Sichelschmidt, J. Ferstl, C. Krellner, C. Geibel, F. Steglich, Phys. Rev. B **74**, 132408 (2006)
[62] T. Park, J.D. Thompson, New. J. Phys. **11**, 055062 (2009)
[63] Q. Si, Physica B: Condensed Matter **378-380**, 23 (2006)
[64] C. Petrovic, P.G. Pagliuso, M.F. Hundley, R. Movshovich, J.L. Sarrao, J.D. Thompson, Z. Fisk, P. Monthoux, J. Phys. Condens. Matter **13**, L337 (2001)
[65] R. Movshovich, M. Jaime, J.D. Thompson, C. Petrovic, Z. Fisk, P.G. Pagliuso, J.L. Sarrao, Phys. Rev. Lett. **86**, 5152 (2001)
[66] J. D. Thompson, Z. Fisk, J. Phys. Soc. Jpn. **81**, 011002 (2012)
[67] C. Petrovic, R. Movshovich, M. Jaime, P.G. Pagliuso, M.F. Hundley, J.L. Sarrao, Z. Fisk, J.D. Thompson, EPL **53**, 354 (2001)
[68] Y. Chen, W.B. Jiang, C.Y. Guo, F. Ronning, E.D. Bauer, T. Park, H.Q. Yuan, Z. Fisk, J.D. Thompson, X. Lu, Phys. Rev. Lett. **114**, 146403 (2015)
[69] M.D. Bachmann, G.M. Ferguson, F. Theuss, T. Meng, C. Putzke, T. Helm, K. Shirer, Y.S. Li, K. Modic, M. Nicklas, M. König, D. Low, S. Ghosh, A.P. Mackenzie, F. Arnold, E. Hassinger, R.D. McDonald, L.E. Winter, E.D. Bauer, F. Ronning, B. Ramshaw, K.C. Nowack, P.J. Moll, Spatially modulated heavy-fermion superconductivity in $CeIrIn_5$ (2018). ArXiv:1807.05079
[70] S.I. Fujimori, T. Okane, J.Okamoto, K. Mamiya, Y. Muramatsu, Phys. Rev. B **67**, 144507 (2003)
[71] S.i. Fujimori, A. Fujimori, K. Shimada, T. Narimura, K. Kobayashi, H. Namatame, M. Taniguchi,

H. Harima, H. Shishido, S. Ikeda, D. Aoki, Y. Tokiwa, Y. Haga, Y. Ōnuki, Phys. Rev. B **73**, 224517 (2006)

[72] Q.Y. Chen, C.H.P. Wen, Q. Yao, K. Huang, Z.F. Ding, L. Shu, X.H. Niu, Y. Zhang, X.C. Lai, Y.B. Huang, G.B. Zhang, S. Kirchner, D.L. Feng, Phys. Rev. B **97**, 075149 (2018)

[73] S. Wirth, Y. Prots, M. Wedel, S. Ernst, S. Kirchner, Z. Fisk, J.D. Thompson4, F. Steglich, Y. Grin, J. Phys. Soc. Jpn. **83**, 061009 (2014)

[74] A. Koitzsch, S.V. Borisenko, D. Inosov, J. Geck, V.B. Zabolotnyy, H. Shiozawa, M. Knupfer, J. Fink, B. Büchner, E.D. Bauer, J.L. Sarrao, R. Follath, Phys. Rev. B **77**, 155128 (2008)

[75] A. Koitzsch, I. Opahle, S. Elgazzar, S.V. Borisenko, J. Geck, V.B. Zabolotnyy, D. Inosov, H. Shiozawa, M. Richter, M. Knupfer, J. Fink, B. Büchner, E.D. Bauer, J.L. Sarrao, R. Follath, Phys. Rev. B **79**, 075104 (2009)

[76] A. Koitzsch, T.K. Kim, U. Treske, M. Knupfer, B. Büchner, M. Richter, I. Opahle, R. Follath, E.D. Bauer, J.L. Sarrao, Phys. Rev. B **88**, 035124 (2013)

[77] E.J. Singley, D.N. Basov, E.D. Bauer, M.B. Maple, Phys. Rev. B **65**, 161101(R) (2002)

[78] K.S. Burch, S.V. Dordevic, F.P. Mena, A.B. Kuzmenko, D. van der Marel, J.L. Sarrao, J.R. Jeffries, E.D. Bauer, M.B. Maple, D.N. Basov, Phys. Rev. B **75**, 054523 (2007)

[79] P. Aynajian, E.H. da Silva Neto, A. Gyenis, R.E. Baumbach, J.D. Thompson, Z. Fisk, E.D. Bauer, A. Yazdani, Mature **486**, 201 (2012)

[80] M.P. Allan, F. Massee, D.K. Morr, J.V. Dyke, A.W. Rost, A.P. Mackenzie, C. Petrovic, J.C. Davis, Nature Phys. **9**, 468 (2013)

[81] B.B. Zhou, S. Misra, E.H. da Silva Neto, P. Aynajian, R.E. Baumbach, J.D. Thompson, E.D. Bauer, A. Yazdani, Nature Phys. **9**, 474 (2013)

[82] R. Settai, H. Shishido, S. Ikeda, Y. Murakawa, M. Nakashima, D. Aoki, Y. Haga, H. Harima, Y. Onuki, J. Phys. Condens. Matter **13**, L627 (2001)

[83] H. Shishido, R. Settai, D. Aoki, S. Ikeda, H. Nakawaki, N. Nakamura, T. Iizuka, Y. Inada, K. Sugiyama, T. Takeuchi, K. Kindo, T.C. Kobayashi, Y. Haga, H. Harima, Y. Aoki, T. Namiki, H. Sato, Y. Ōnuki, J. Phys. Soc. Jpn. **71**, 162 (2002)

[84] K. Haule, C.H. Yee, K. Kim, Phys. Rev. B **81**, 195107 (2010)

[85] F. Ronning, C. Capan, A. Bianchi, R. Movshovich, A. Lacerda, M.F. Hundley, J.D. Thompson, P.G. Pagliuso, J.L. Sarrao, Phys. Rev. B **71**, 104528 (2005)

[86] S. Singh, C. Capan, M. Nicklas, M. Rams, A. Gladun, H. Lee, J.F. DiTusa, Z. Fisk, F. Steglich, S. Wirth, Phys. Rev. Lett. **98**, 057001 (2007)

[87] S. Zaum, K. Grube, R. Schäfer, E.D. Bauer, J.D. Thompson, H. v. Löhneysen, Phys. Rev. Lett. **106**, 087003 (2011)

[88] S. Pal, C. Wetli, F. Zamani, O. Stockert, H. von Löhneysen, M. Fiebig, J. Kroha, Fermi surface evolution and crystal field excitations in heavy-fermion compounds probed by time-domain terahertz spectroscopy (2018). ArXiv:1810.07412

[89] S.K. Mo, W.S. Lee, F. Schmitt, Y.L. Chen, D.H. Lu, C. Capan, D.J. Kim, Z. Fisk, C.Q. Zhang, Z. Hussain, Z.X. Shen, Phys. Rev. B **85**, 241103(R) (2012)

[90] S. Jang, J.D. Denlinger, J.W. Allen, V.S. Zapf, M.B. Maple, J.N. Kim, B.G. Jang, J.H. Shim, Evolution of the Kondo lattice electronic structure above the transport coherence temperature (2017). ArXiv:1704.08247

[91] Q.Y. Chen, D.F. Xu, X.H. Niu, R. Peng, H.C. Xu, C.H.P. Wen, X. Liu, L. Shu, S.Y. Tan, X.C. Lai, Y.J. Zhang, H. Lee, V.N. Strocov, F. Bisti, P. Dudin, J.X. Zhu, H.Q. Yuan, S. Kirchner, D.L. Feng, Phys. Rev. Lett. **120**, 066403 (2018)

[92] E.H. da Silva Neto, P. Aynajian, R.E. Baumbach, E.D. Bauer, J. Mydosh, S. Ono, A. Yazdani, Phys. Rev. B **87**, 161117 (2013)

[93] D. Huang, C.L. Song, T.A. Webb, S. Fang, C.Z. Chang, J.S. Moodera, E. Kaxiras, J.E. Hoffman, Phys. Rev. Lett. **115**, 017002 (2015)

[94] P. Aynajian, E.H. da Silva Neto, B.B. Zhou, S. Misra, R.E. Baumbach, Z. Fisk, J. Mydosh, J.D. Thompson, E.D. Bauer, A. Yazdani, J. Phys. Soc. Jpn. **83**, 061008 (2014)

[95] M. Haze, Y. Torii, R. Peters, S. Kasahara, Y. Kasahara, T. Shibauchi, T. Terashima, Y. Matsuda, J. Phys. Soc. Jpn. **87**, 034702 (2018)
[96] H. Shishido, R. Settai, H. Harima, Y. Ōnuki, J. Phys. Soc. Jpn. **74**, 1103 (2005)
[97] H. Hegger, C. Petrovic, E.G. Moshopoulou, M.F. Hundley, J.L. Sarrao, Z. Fisk, J.D. Thompson, Phys. Rev. Lett. **84**, 4986 (2000)
[98] F.P. Mena, D. van der Marel, J.L. Sarrao, Phys. Rev. B **72**, 045119 (2005)
[99] D.P. Moore, T. Durakiewicz, J.J. Joyce, A.J. Arko, L.A. Moralesa, J.L. Sarrao, P.G. Pagliuso, J.M. Wills, C.G. Olson, Physica B **312-313**, 134 (2002)
[100] M. Haze, R. Peters, Y. Torii, T. Suematsu, D.S.M. Naritsuka, Y. Kasahara, T. Shibauchi, T. Terashima, Y. Matsuda, J. Phys. Soc. Jpn. **88**, 014706 (2019)
[101] R.Y. Chen, N.L. Wang, Rep. Prog. Phys. **79**, 064502 (2016)
[102] F. Marabelli, P. Wachter, Phys. Rev. B **42**, 3307 (1990)
[103] M. Klein, A. Nuber, F. Reinert, J. Kroha, O. Stockert, H. v. Löhneysen, Phys. Rev. Lett. **101**, 266404 (2008)
[104] C. Wetli, S. Pal, J. Kroha, K. Kliemt, C. Krellner, O. Stockert, H. v. Löhneysen, M. Fiebig, Nature Phys. **14**, 1103 (2018)
[105] O. Trovarelli, C. Geibel, S. Mederle, C. Langhammer, F.M. Grosche, P. Gegenwart, M. Lang, G. Sparn, F. Steglich, Phys. Rev. Lett. **85**, 626 (2000)
[106] P. Gegenwart, Y. Tokiwa, T. Westerkamp, F. Weickert, J. Custers, J. Ferstl, C. Krellner, K.H.M. C. Geibel P. Kersch and, F. Steglich, New J. Phys. **8**, 171 (2006)
[107] M. Taupin, G. Knebel, T.D. Matsuda, G. Lapertot, Y. Machida, K. Izawa, J.P. Brison, J. Flouquet, Phys. Rev. Lett. **115**, 046402 (2015)
[108] J. Paglione, T.A. Sayles, P.C. Ho, J.R. Jeffries, M.B. Maple, Nature Phys. **3**, 703 (2007)
[109] T. Park, V.A. Sidorov, F. Ronning, J.X. Zhu, Y. Tokiwa, H. Lee, E.D. Bauer, R. Movshovich, J.L. Sarrao, J.D. Thompson, Nature **456**, 366 (2008)
[110] A. Amato, D. Jaccard, J. Flouquet, F. Lapierre, J.L. Tholence, R.A. Fisher, S.E. Lacy, J.A. Olsen, N.E. Phillips, J. Low Temp. Phys. **68**, 371 (1987)
[111] H.E. Fischer, E.T. Swartz, R.O. Pohl, B.A. Jones, J.W. Wilkins, Z. Fisk, Phys. Rev. B **36**, 5330 (1987)
[112] H.v. Löhneysen, T. Pietrus, G. Portisch, H.G. Schlager, A. Schröder, M. Sieck, T. Trappmann, Phys. Rev. Lett. **72**, 3262 (1994)
[113] V.A. Sidorov, M. Nicklas, P.G. Pagliuso, J.L. Sarrao, Y. Bang, A.V. Balatsky, J.D. Thompson, Phys. Rev. Lett. **89**, 157004 (2002)
[114] L.D. Pham, T. Park, S. Maquilon, J.D. Thompson, Z. Fisk, Phys. Rev. Lett. **97**, 056404 (2006)
[115] L. Petersen, P.T. Sprunger, P. Hofmann, E. Lægsgaard, B.G. Briner, M. Doering, H.P. Rust, A.M. Bradshaw, F. Besenbacher, E.W. Plummer, Phys. Rev. B **57**, R6858 (1998)
[116] L. Petersen, P. Hofmann, E. Plummer, F. Besenbacher, J. Electron Spectros. and Relat. Phenom. **109**, 97 (2000)
[117] F.P. Toldin, J. Figgins, S. Kirchner, D.K. Morr, Phys. Rev. B **88**, 081101(R) (2013)
[118] H. Shishido, T. Shibauchi, K. Yasu, T. Kato, H. Kontani, T. Terashima, Y. Matsuda, Science **327**(5968), 980 (2010)
[119] S. Kirchner, Q. Si, Phys. Rev. Lett. **103**, 206401 (2009)
[120] P. Ribeiro, F. Zamani, S. Kirchner, Phys. Rev. Lett. **115**, 220602 (2015)
[121] F. Zamani, P. Ribeiro, S. Kirchner, J. Magn. Magn. **400**, 7 (2016)
[122] P. Gegenwart, Q. Si, F. Steglich, Nat. Phys. **4**, 186 (2008)
[123] Q. Si, S. Paschen, Phys. Status Solidi B **250**, 425 (2013)
[124] G.R. Stewart, Rev. Mod. Phys. **73**, 797 (2001)
[125] S. Wu, W.A. Phelan, L. Liu, J.R. Morey, J.A. Tutmaher, J.C. Neuefeind, A. Huq, M.B. Stone, M. Feygenson, D.W. Tam, B.A. Frandsen, B. Trump, C. Wan, S.R. Dunsiger, T.M. McQueen, Y.J. Uemura, C.L. Broholm, Phys. Rev. Lett. **122**, 197203 (2019)
[126] Y. Luo, L. Pourovskii, S.E. Rowley, Y. Li, C. Feng, A. Georges, J. Dai, G. Cao, Z. Xu, Q. Si,

N.P. Ong, Nat. Mater. **13**, 777 (2014)
[127] A. Crepaldi, S. Pons, E. Frantzeskakis, F. Calleja, M. Etzkorn, A.P. Seitsonen, K. Kern, H. Brune, M. Grioni, Phys. Rev. B **87**, 115138 (2013)
[128] N. Nicoara, E. Román, J.M. Gómez-Rodriguez, J.A. Martin-Gago, J. Méndez, Organic Electr. **7**, 287 (2006)
[129] R.S. Markiewicz, Phys. Rev. B **69**, 214517 (2004)
[130] K.M. Shen, J.S. Davis, Materials Today **11**(9), 14 (2008)